

Quantum Critical Points and the Sign Problem

R. Mondaini,^{1,*} S. Tarat,^{1,†} and R.T. Scalettar^{2,‡}

¹*Beijing Computational Science Research Center, Beijing 100193, China*

²*Department of Physics, University of California, Davis, CA 95616, USA*

The “sign problem” (SP) is the fundamental limitation to simulations of strongly correlated materials in condensed matter physics, solving quantum chromodynamics at finite baryon density, and computational studies of nuclear matter. As a result, it is part of the reason fields such as ultra-cold atomic physics are so exciting: they can provide quantum emulators of models that could not otherwise be solved, due to the SP. For the same reason, it is also one of the primary motivations behind quantum computation. It is often argued that the SP is not intrinsic to the physics of particular Hamiltonians, since the details of how it onsets, and its eventual occurrence, can be altered by the choice of algorithm or many-particle basis. Despite that, we show that the SP in determinant quantum Monte Carlo (DQMC) is quantitatively linked to quantum critical behavior. We demonstrate this via simulations of a number of fundamental models of condensed matter physics, including the spinful and spinless Hubbard Hamiltonians on a honeycomb lattice and the ionic Hubbard Hamiltonian, all of whose critical properties are relatively well understood. We then propose a reinterpretation of the low average sign for the Hubbard model on the square lattice when away from half-filling, an important open problem in condensed matter physics, in terms of the onset of pseudogap behavior and exotic superconductivity. Our study charts a path for exploiting the average sign in QMC simulations to understand quantum critical behavior, rather than solely as an obstacle that prevents quantum simulations of many-body Hamiltonians at low temperature.

Over the last several decades, quantum Monte Carlo (QMC) simulations have provided great insight into challenging strong correlation problems in chemistry [1, 2], condensed matter [3, 4], nuclear [5], and high energy physics [6]. In all these areas, however, the sign problem (SP), which occurs when the probability for specific quantum configurations in the importance sampling becomes negative, significantly constrains their application. Solving, or at least mitigating, the SP is one of the central endeavors of computational physics. The extent and importance of the effort is indicated by the many proposed solutions, and their continued development over the last three decades — see the Supplemental Materials (SM) for a review [7].

Despite enormous effort, the SP remains unsolved. In fact, the lack of progress is one of the main driving forces behind a number of large-scale efforts, including the quest for quantum emulators [8–10] as well as quantum computing itself [11, 12]. One of the most fundamental mysteries concerns the possible link between the sign problem and the underlying physics of the Hamiltonian being investigated.

Here, instead of challenging this NP-hard problem [13], or proposing solutions that can partially ameliorate its behavior [14, 15] we show that there is a clear *quantitative* connection between the behavior of the average sign $\langle \mathcal{S} \rangle$ in the widely used Determinant Quantum Monte Carlo (DQMC) method and several quantum phase transitions: that of the semimetal to antiferromagnetic Mott insulator (AFMI) of Dirac fermions in the spinful [SU(2)] honeycomb-Hubbard Hamiltonian [16, 17], the band to correlated insulator transition [18–20], and charge density wave transitions of spinless [U(1)] fermions on a hon-

eycomb lattice [21, 22]. In the first case, simulations at half-filling, where the quantum critical point (QCP) occurs, are SP free. We introduce a small doping μ and show, in the limit $\mu \rightarrow 0^+$ at temperature $T \rightarrow 0$, that $\langle \mathcal{S} \rangle$ evolves rapidly as we tune through the QCP.

Our second illustration, the ionic Hubbard model, has a SP even at half-filling. Here the average sign undergoes an abrupt drop at the band-insulator (BI) to correlated metal (CM) transition. The third case, spinless fermions on a honeycomb lattice, also has a semimetal to (charge) insulator transition. Its interest relies on the existence of a SP-free approach. Studying it with a method which contains an ‘unnecessary’ SP lends insight into the key question of the algorithm dependence of links between the SP and the physics of model Hamiltonians.

These three discussions establish a link between known physics of the models and the fermion sign. Having made that connection, we then turn to the iconic square lattice Hubbard model whose physics has *not* been conclusively established. We find that the *onset* of the SP occurs in a dome-shaped region of the filling-temperature phase space underneath that of the pseudogap (PG) physics. The SP is well-enough controlled in the PG phase to obtain reliable results for various observables, including the pairing correlations in various channels, exhibiting dominant enhancement for *d*-wave symmetry. Because it onsets exponentially in inverse temperature, the SP provides a rather sharp demarcation of the regime, which mimics the superconducting dome of the cuprates [23]. Although the SP prevents DQMC from resolving a signal of a *d*-wave transition, the ground work established for the honeycomb lattice and BI-CM models suggests that this sign problem dome might be linked to the onset of a

superconducting phase. In the conclusions we will make connections which will further corroborate the generality of our results to other models and QMC methods.

The Sign Problem; Model and Methodology

The origin of the sign problem can be understood in two related classes of algorithms, ‘world-line’ Quantum Monte Carlo (WLQMC) [24] and Green’s function Quantum Monte Carlo (GFQMC) [25, 26], by considering Feynman’s path integral approach, which provides a mapping of quantum statistical mechanics in D dimensions to classical statistical mechanics in $D + 1$ dimensions. Paralleling Feynman’s original exposition for the operator $e^{-i\hat{H}t/\hbar}$, the imaginary time evolution operator $e^{-\beta\hat{H}}$ is subdivided into L_τ incremental pieces $\hat{U}_{\Delta\tau} = e^{-\Delta\tau\hat{H}}$, where $L_\tau \Delta\tau = \beta$, the inverse temperature. Complete sets of states $\hat{\mathcal{L}}_\tau = \sum_{S_\tau} |S_\tau\rangle\langle S_\tau|$ are introduced between each $\hat{U}_{\Delta\tau}$ so that the partition function $\mathcal{Z} = \text{Tr} e^{-\beta\hat{H}}$ becomes a sum over the *classical* degrees of freedom associated with the spatial labels of each $\hat{\mathcal{L}}_\tau$, and also an additional imaginary time index denoting the location $\tau = 1, 2, \dots, L_\tau$ of $\hat{\mathcal{L}}_\tau$ in the string of operators $\hat{U}_{\Delta\tau}$. The quantity being summed in the calculation of \mathcal{Z} is the product of matrix elements $\langle S_\tau | \hat{U}_{\Delta\tau} | S_{\tau+1} \rangle$.

In such WLQMC/GFMC methods, the SP arises when $\prod_\tau \langle S_\tau | \hat{U}_{\Delta\tau} | S_{\tau+1} \rangle < 0$. Negative matrix elements are unavoidable for itinerant fermionic models in $D > 1$ because their sign depends on the number of fermions intervening between two particles undergoing exchange, and hence changes as the particle positions are updated. The basis dependence of the sign problem is apparent by considering intermediate states $|S_\tau\rangle$ chosen to be eigenstates $|\phi_\alpha\rangle$ of \hat{H} . In that case the matrix elements are just $e^{-\Delta\tau E_\alpha}$ and hence are trivially positive definite. Of course, since the eigenstates of \hat{H} are unknown, this is not a practical choice in any non-trivial situation. Moreover, the SP can generally be avoided for bosonic or spin models as long as the lattice is bipartite. Nonetheless, even bosonic and spin Hamiltonians can have negative matrix elements on frustrated geometries [27], especially for antiferromagnetic models, emphasizing the SP is not solely a consequence of Fermi statistics.

‘Auxiliary field’ Quantum Monte Carlo (AFQMC) algorithms [28–30] typically have a much less severe SP than WLQMC [7, 31]. They are based on the observation that the trace of an exponential of a quadratic form of fermionic operators can be done analytically, resulting in the determinant of a matrix of dimension set by the cardinality of fermionic operators. The determinant is the product $\prod_j (1 + e^{-\beta\varepsilon_j})$, where ε_j are the non-interacting energy levels, and is always positive.

If interactions are present, quartic terms in \hat{H} are reduced to quadratic ones with a Hubbard-Stratonovich (HS) transformation. The trace of the resulting product of exponentials of quadratic forms can be performed, but

now they each depend on a different, i.e. imaginary-time dependent, auxiliary field. The resulting determinant is no longer guaranteed to be positive; the consequence is the SP since the HS field needs to be sampled stochastically in order to compute operator expectation values.

In AFQMC, the trace over fermionic degrees of freedom is done for all species (i.e. all spin and orbital indices α). If there is no hybridization between different α , each trace gives an individual determinant. In some situations, particle-hole, time-reversal, or other symmetries [32–34] impose a relation between the determinants for different α ’s, and as a consequence the negative determinants always come in pairs. Low temperature (ground-state) properties can be accessed in such ‘sign problem free’ cases, and a host of interesting quantum phase transitions has been explored [35–38]. If such a partnering does not occur, a reasonable rule of thumb is that the average sign $\langle \mathcal{S} \rangle$ is sufficiently bounded away from zero with measurements that exhibit sufficiently small error bars for $T \gtrsim W/20 - W/40$, at intermediate interaction strengths (of the same order as the bandwidth W) [39].

The DQMC methodology [28, 29] we use is a specific implementation of AFQMC. We employ the discrete HS transformation introduced by Hirsch [40] and choose the Trotter discretization $\Delta\tau$ such that systematic errors in $\langle \mathcal{S} \rangle$ and other observables are of the same order as statistical sampling errors. (See [7] for additional details.)

We mostly consider models in which two (spin) species of itinerant electrons hop on a lattice with an on-site repulsion, i.e., variants of the Hubbard Hamiltonian,

$$\hat{H} = - \sum_{ij\sigma} t_{ij} (\hat{c}_{i\sigma}^\dagger \hat{c}_{j\sigma} + \hat{c}_{j\sigma}^\dagger \hat{c}_{i\sigma}) - \sum_{i\sigma} \mu_i \hat{n}_{i\sigma} + U \sum_i \left(\hat{n}_{i\uparrow} - \frac{1}{2} \right) \left(\hat{n}_{i\downarrow} - \frac{1}{2} \right). \quad (1)$$

Here $\hat{c}_{j\sigma}^\dagger$ ($\hat{c}_{j\sigma}$) are creation (destruction) operators at site i with spin σ and $\hat{n}_{i\sigma} = \hat{c}_{i\sigma}^\dagger \hat{c}_{i\sigma}$ is the number operator. In Sec. I, i, j are near-neighbor sites on a honeycomb lattice, with $t_{ij} = t$. As a consequence of particle-hole symmetry (PHS), $\mu_i = 0$ corresponds to half-filling, and $\rho = \langle \hat{n}_{i\sigma} \rangle = 1/2$, for arbitrary U and temperature T . In Sec. II, we consider a $t_{ij} = t$ square lattice with $\mu_i = +\Delta$ on one sublattice and $\mu_i = -\Delta$ on the other, a situation which has a SP even at half-filling, but which is mild enough to allow its phase diagram to be established with reasonable reliability. Sec. III concerns a single species model with interactions between fermions on neighboring sites, notable because a SP-free QMC formulation exists [22, 41].

All these models have QCPs which have been located to fairly high precision and so serve as testbeds for demonstrating that the average sign can be used as an alternate means to study the onset of quantum criticality. In our final investigation, Sec. IV, we consider the doped, spinful, square lattice Hubbard model, much of

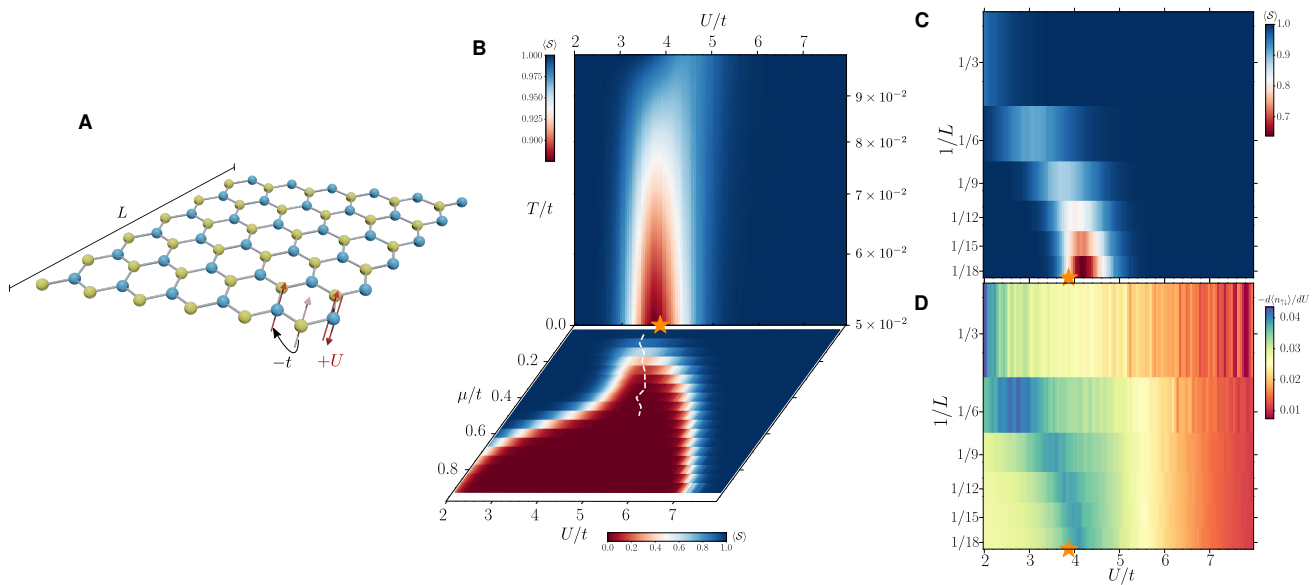


Figure 1. **The SU(2) Hubbard model on the honeycomb lattice.** (A) Cartoon depicting a honeycomb lattice with $N = 2L^2$ sites ($L = 6$ here), accompanied by the relevant terms in \hat{H} . (B) Contour plot of the average $\langle S \rangle$ in the T/t (μ/t) vs U/t in the upper (lower) panel. Here $L = 9$ and $\mu/t = 0.1$ ($T/t = 1/20$) in the upper (lower) panel. (C) The average sign extrapolated with the linear system size L , using $T/t = 1/20$ and $\mu/t = 0.1$. (D) Similar extrapolation as in C, but displaying a local quantity (the derivative of the double occupancy), which is an indicator of the QCP. In all panels with data, the prediction for the ground-state phase transition occurring at $U_c/t = 3.869$ [17] is depicted by a star marker.

whose low temperature physics remains shrouded in mystery. We correlate the behavior of the SP with some of its properties at intermediate temperature, and then describe what might be inferred concerning one of the most elusive puzzles—the presence of a low temperature superconducting dome.

I. Semimetal to AFMI on a Honeycomb Lattice

On a honeycomb lattice (Fig. 1A), the $U = 0$ Hubbard Hamiltonian has a semi-metallic density of states which vanishes linearly at $E = 0$. Its dispersion relation $E(\mathbf{k})$ has Dirac points in the vicinity of which the kinetic energy varies linearly with momentum. Unlike the square lattice that displays AF order for all $U \neq 0$, the honeycomb Hubbard model at $T \rightarrow 0$ remains a semimetal for small nonzero U , turning to an AF insulator only for U exceeding a critical U_c . Early DQMC and series expansion calculations estimated $U_c \sim 4t$ [42], with subsequent studies [16, 17] yielding the more precise value $U_c/t = 3.869$.

The upper panel of Fig. 1B gives $\langle S \rangle$ in the U - T plane. By introducing a small non-zero $\mu = 0.1$, we can induce a SP which begins to develop at $T/t \sim 0.1$. As T is lowered further the average sign deviates from $\langle S \rangle = 1$ in a relatively narrow window of U/t close to the known U_c . In turn, we show the $\langle S \rangle$ on the $U - \mu$ plane at fixed $T/t = 0.05$ in the lower panel of Fig. 1B. For large μ the sign is small for a broad swath of interaction values. As μ decreases this region pinches down until it terminates

close to U_c ; the dashed white line displays the minimum $\langle S \rangle$ in the relevant range. In both panels, the behavior of the average sign outlines the quantum critical fan that extends above the QCP.

Figure 1C shows a finite size extrapolation of $\langle S \rangle$ in the $1/L - U$ plane, where L is the linear lattice size. Just as $\langle S \rangle$ worsens with increasing β , it is also known to deviate increasingly from $\langle S \rangle = 1$ with growing L [29]. What these data further indicate is that the extrapolation $L \rightarrow \infty$ clearly reveals U_c in the presence of a small chemical potential. So far, we have exclusively used $\langle S \rangle$ in locating U_c . Original investigations employed more ‘traditional’ (and more physical) correlation functions such as the AF structure factor and conductivity. For comparison to the evolution of $\langle S \rangle$, Fig. 1D shows one example, the rate of change of the double occupancy D , again in the $1/L - U$ plane. A peak in $-dD/dU$ indicates where local moments $\langle m^2 \rangle$ are growing most rapidly. The similarity between Figs. 1C and 1D emphasizes how $\langle S \rangle$ is tracking the physics of the model in a way remarkably similar to $\langle m^2 \rangle$. The combination of the three limits, μ, β, L , unequivocally points out the QCP location; the SM [7] contains further discussion, and other observables.

II. Ionic Hubbard BI to AF Transition

Among the different types of non-conducting states are ‘band insulators’ (BI), in which the chemical potential lies in a gap in the non-interacting density of states (DOS), and ‘Mott insulators’ (MI) in which strong re-

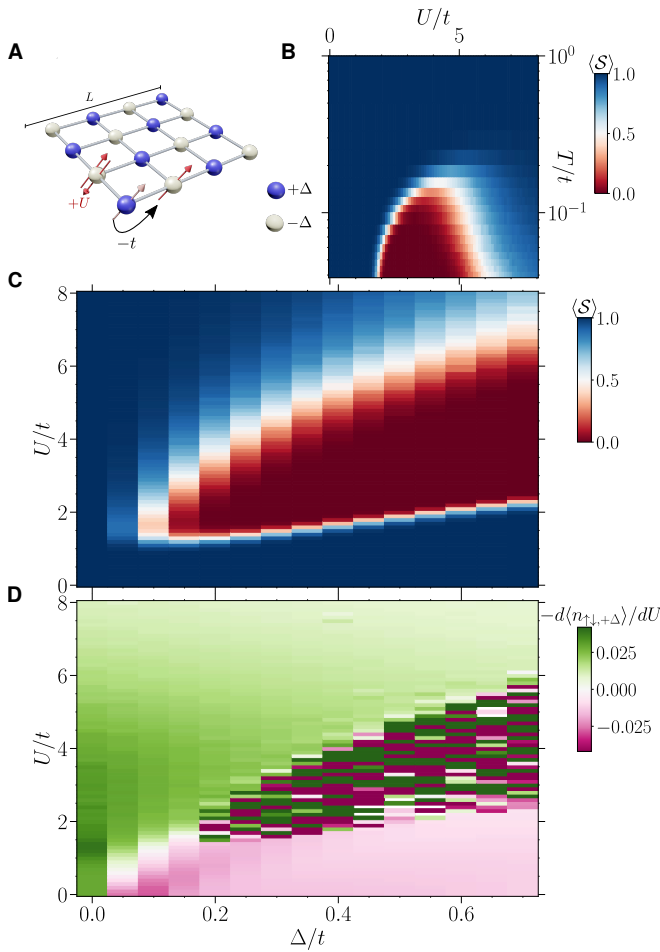


Figure 2. **The SU(2) Ionic Hubbard model on the square lattice.** (A) Cartoon depicting a square lattice with $N = L^2$ sites ($L = 4$ here), accompanied by the relevant terms in \hat{H} . (B) Contour plot of the average $\langle S \rangle$ in the U/t vs. T/t plane, with staggered potential $\Delta/t = 0.5$. (C) The contour of $\langle S \rangle$ as function of the competing parameters U/t and Δ/t , at a temperature $T/t = 1/24$. (D) The corresponding derivative of the double occupancy on the $+\Delta$ sites at the same parameters as in C. In all data, Trotter discretization is chosen as $\Delta\tau = 0.1$ and the lattice size is $L = 12$.

pulsive interactions prevent hopping at commensurate filling. The evolution from BI to MI is a fascinating issue in condensed matter physics [18–20, 44–46]. In the ionic Hubbard model we investigate here, a staggered site energy $\mu_i = \pm\Delta$ on the two sublattices of a square lattice (Fig. 2A) leads to a dispersion relation $E(k) = \pm\sqrt{\varepsilon(k)^2 + \Delta^2}$ with $\varepsilon(k) = -2t(\cos k_x + \cos k_y)$. The resulting DOS vanishes in the range $-\Delta < E < +\Delta$ in which the lattice is half-filled, resulting in a BI. The occupation of the ‘low energy’ sites $\mu_i = -\Delta$ is greater than that of the ‘high energy’ sites $\mu_i = +\Delta$, so that there is a trivial charge density wave (CDW) order associated with an explicit breaking of the sublattice symmetry in the Hamiltonian.

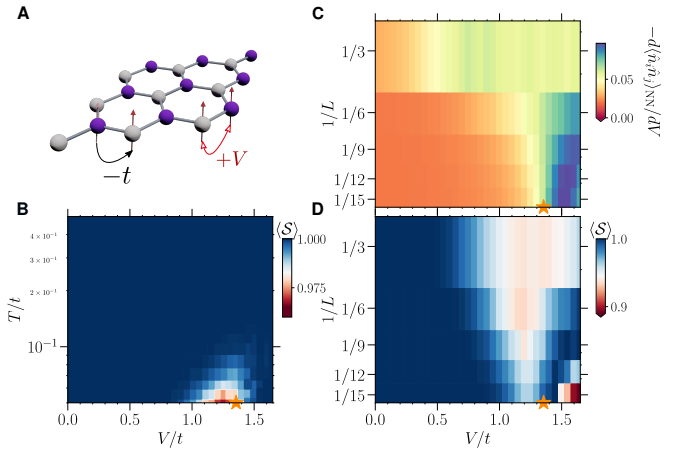


Figure 3. **The U(1) Hubbard model on the honeycomb lattice.** (A) Schematics of the spinless fermion Hamiltonian [Eq. (2)] with nearest-neighbor interaction on a lattice with $L = 3$. Temperature extrapolation of the average $\langle S \rangle$ as function of the nearest-neighbor interaction V/t , for a lattice with $L = 9$. (D) [(C)] Extrapolation of the average sign [derivative of the nearest-neighbor correlation in respect to V] with the inverse of the linear size L along a range of interactions, at a temperature T that scales with the system size $T/t = 0.0375/L\Delta\tau$. Here $\langle S \rangle$ marginally increases when tackling larger sizes, indicating that the dynamical critical exponent z in the scaling with $L\tau/L^z$ is larger than one [7, 43]; we used $z = 1$ above. In all data, Trotter discretization is chosen as $\Delta\tau = 0.1$. As for the SU(2) case, the star marker depicts the best known value of the interactions that trigger the Mott insulating phase; here with CDW order at the ground-state [41].

An onsite repulsion U disfavors this density modulation: The potential energy $Un_{i\uparrow}n_{i\downarrow}$ is higher than for a uniform occupation. Thus the driving physics of the BI, the staggered site energy Δ and that of the MI, the repulsion U , are in competition. Although the simplest scenario is a direct BI to MI transition with increasing U , one of the more exotic possible outcomes is the emergence of a metallic phase when these two energy scales are in balance and neither type of insulator can dominate the behavior. Past DQMC simulations suggest this less trivial case occurs, and have used the temperature dependence of the dc conductivity to bound the metallic phase [46, 47].

Here we investigate how this physics might be reflected in the average sign. Figure 2B shows $\langle S \rangle$ in the U/t – T/t plane at $\Delta = 0.5t$. As T is lowered, $\langle S \rangle$ deviates from unity for a range of intermediate U values. Figure 2C gives the behavior in the U/t – Δ/t plane at fixed low $T = t/24$. The central result is that $\langle S \rangle$ is small in a region which maps well with the previously determined boundaries of the metallic phase [46, 47]. This is emphasized by a comparison to Fig. 2D, which uses one of the ‘traditional’ methods for phase boundary location, namely the behavior of the double occupancy. The BI

has a low occupancy, and hence very low double occupancy on the $+\Delta$ -sites. Increasing U smooths out the density, so that the double occupancy on the $+\Delta$ -sites *increases*: $d\langle n_{\uparrow\downarrow,+\Delta} \rangle/dU > 0$. In contrast, in the MI region, $U \gtrsim \Delta$, the physics is that of the usual Hubbard Hamiltonian and double occupancy *decreases* as U grows: $d\langle n_{\uparrow\downarrow,+\Delta} \rangle/dU < 0$.

In the CM region between BI and MI, however, obtaining a relevant signal-to-noise ratio for the traditional observables is exponentially challenging precisely because the average sign vanishes in this region. The ‘phase diagram’ obtained by $\langle \mathcal{S} \rangle$ (Fig. 2 C) is remarkably similar to that given by the physical observable, the rate of change of double occupancy with U (Fig. 2 D)

As in the determination of the QCP for the spinful Hubbard model on a honeycomb lattice, $\langle \mathcal{S} \rangle$ emerges as more than a mere nuisance, but as a harbinger of the physics. An in-depth similarity between these two situations is discussed in the SM [7], where we show that the BI-metal QCP is again uniquely identified by the $1/L$ scaling of $\langle \mathcal{S} \rangle$, in precise analogy with the honeycomb case. These results suggest the existence of a quantum critical region associated with the CM phase and the vanishing $\langle \mathcal{S} \rangle$.

III. An ‘Unnecessary’ Sign Problem

We now consider spinless fermions, where the on-site Hubbard interaction U , made irrelevant by the Pauli principle, is replaced by an intersite repulsion V ,

$$\hat{H} = -t \sum_{\langle ij \rangle} (\hat{c}_i^\dagger \hat{c}_j + \hat{c}_j^\dagger \hat{c}_i) + V \sum_{\langle ij \rangle} \hat{n}_i \hat{n}_j. \quad (2)$$

Equation 2 provides an example of a model where the SP can be completely solved by utilizing special techniques such as the fermion bag in the Continuous Time QMC approach [35], or by going to a different basis employing a Majorana representation of the fermions in the AFQMC method [41], as long as the system is on a bipartite lattice and $V > 0$. The standard Blankenbecler, Scalapino, and Sugar (BSS) approach [28], on the other hand, manifestly displays a SP in the low temperature regime. Nevertheless, in order to study the sign and its connection with the underlying physics, we use a BSS based algorithm to investigate the system on a honeycomb lattice (Fig. 3 A). Consideration of this ‘unnecessary’ SP allows us to address fundamental issues related to the algorithm dependence of links between the SP and the physics of model Hamiltonians.

At $T = 0$, the model displays a QPT between a Dirac semimetal and an insulating staggered CDW state as the interaction is tuned through a critical value V_c [22]. At large V , the repulsive interaction favours a CDW state, distinguished from that of the ionic Hubbard model by the fact that there is no staggered external field here – the

CDW phase is a result of *spontaneous* symmetry breaking. As V is reduced, increasing quantum fluctuations due to hopping finally destroy the CDW state, resulting in a Dirac semimetal for $V < V_c$. Accurate estimates based on SP free methods yield $V_c \sim 1.35t$ [41].

In Fig. 3 B, we show a map of the temperature extrapolation of $\langle \mathcal{S} \rangle$ as a function of V . The sign shows a clear reduction around the known V_c (denoted by the star).

Figure 3 D shows the spatial lattice size dependence of the sign, and Fig. 3 C, once again, a more ‘traditional’ local variable, the derivative of the nearest-neighbor (NN) density-density correlation, $\langle n_i n_j \rangle_{\text{NN}}$, with respect to V . In the CDW phase, increasing V strengthens the staggered order, reducing the NN density correlations, and hence $-d\langle n_i n_j \rangle_{\text{NN}}/dV$ is positive. Conversely, the effect is much smaller in the semimetal state, where the derivative is close to zero. The transition V_c is characterized by a clear downturn in this quantity, which becomes progressively sharper as L increases, as Figure 3 C shows. This variable, thus, serves as a physical indicator of the QPT, allowing a comparison of Figs. 3 C,D to demonstrate the connection between the QCP and the behavior of $\langle \mathcal{S} \rangle$. In this model, $\langle \mathcal{S} \rangle$ is well enough behaved that a study of the finite-temperature CDW transition with DQMC is feasible [7], without having to resort to SP-free approaches [48].

IV. Square Lattice Hubbard Model

The essential physics of the cuprate superconductors consists of antiferromagnetic order at and near one hole per CuO_2 cell, a superconducting dome upon doping, which typically extends to densities $0.6 \lesssim \rho \lesssim 0.9$ and a ‘pseudogap’/‘strange metal’ phase above the dome [23, 49]. There are many quantitative, experimentally-based, phase diagrams of different materials which determine the regions occupied by these phases [50]. Likewise, there are computational studies of individual (ρ, T, U) points establishing magnetic/charge order [51], linear resistivity [52], a reduction in the spectral weight for spin excitations [53, 54], and d -wave pairing [55, 56].

Here we reveal a ‘sign problem phase diagram’ which bears significant resemblance to that of experiments. As is well known, the severity of the sign problem itself precludes determination of d -wave order in DQMC via ‘traditional’ observables such as the associated correlation functions. However, Figure 4, based on the behavior of the sign itself, is suggestive. We report the average sign (Fig. 4 A), the enhancement of the d -wave pairing susceptibility over its value in the absence of the pairing vertex [57] (Fig. 4 B), and the uniform, static spin susceptibility $\chi(\mathbf{q} = 0)$ in both the $T/t - \mu/t$ (A–C) and $T/t - \rho$ (D–F) planes – see SM [7].

The most salient features of this ‘sign phase diagram’ are (i) the ‘dome’ of vanishing $\langle \mathcal{S} \rangle$ which occurs in a range of densities $0.4 \lesssim \rho \lesssim 1$ as T is lowered (Fig. 4 D); (ii)

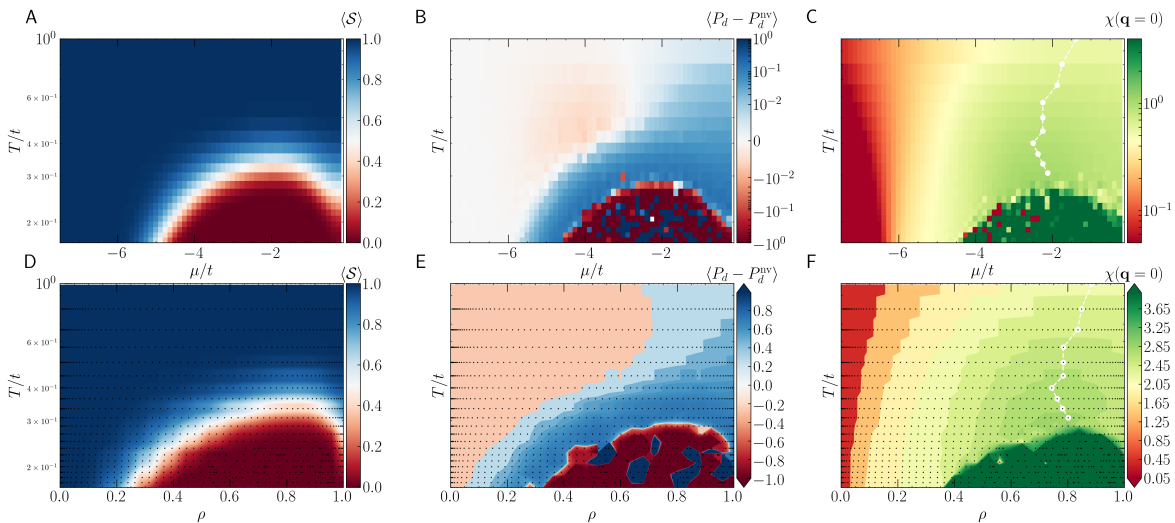


Figure 4. **Square lattice Hubbard model.** (A) Temperature dependence of the average $\langle S \rangle$ as function of the chemical potential μ/t , for a lattice with $L = 16$, $U/t = 6$ and next-near-neighbor hopping $t'/t = -0.2$, values chosen to be close to those in cuprate materials. (B) The d -wave pair susceptibility (subtracted from the non-vertex contribution) for the same parameters. (C) The corresponding static spin susceptibility $\chi(\mathbf{q} = 0)$. The white markers describe its peak for values at which the average sign is large enough to allow a reliable calculation, which encompasses the pseudogap regime. (D, E and F) display the corresponding diagrams when converting to the calculated average density. The black markers depict the actual average density extracted from the regular mesh of μ used in the upper panels, and where an interpolation of the data is performed. In all data, Trotter discretization is chosen as $\Delta\tau = 0.0625$.

the enhancement of d -wave pairing (Fig. 4 E) surrounding the sign dome; and (iii), that the magnetic properties are also linked to the $\langle S \rangle$ -dome: the trajectory tracing the peak value of $\chi(q = 0)$ as T is decreased terminates precisely at the top of the dome (Fig. 4 F). In isolation, the comparisons of the behavior of the sign and the pairing and magnetic responses in the square lattice Hubbard model appear likely to be merely coincidental. Indeed, the fact that the sign is worst precisely for optimal dopings has been previously remarked, but thought to be just ‘bad luck’ [32, 57–59]. However, that the *known* QCP of the three models discussed in Secs. I-III *can* be quantitatively linked to the behavior of $\langle S \rangle$ suggest that the sign dome might actually be indicative of the presence of d -wave superconductivity.

Discussion and Outlook

Early in the history of the study of the sign problem, a simple connection was noted between the fermionic physics and negative weights in auxiliary field QMC: If one artificially constructs two Hubbard-Stratonovich field configurations, one associated with two particle exchanging as they propagate in imaginary time and another with no exchange, one finds that the associated fermion determinants are negative in the former case, and positive in the latter [60]. This interesting observation, however, pertains to low density, that is, to the propagation of just two electrons. Another key observation is that the SP can be viewed as being proportional to the

exponential of the difference of free energy densities of the original fermionic problem, and the one used with the weights in the Monte Carlo sampling taken to be positive, akin to a bosonic formulation of the problem [13, 32]. It highlights how intrinsic the SP is in QMC methods. A last important remark is that ordered phases are often associated with a reduction in the importance of configurations which scramble the sign. This is graphically illustrated in the snapshots of [24]. Although less crisp, similar effects are seen in auxiliary field QMC, for example in considering the evolution from the attractive Hubbard model to the Holstein model with decreasing phonon frequency ω_0 . Reducing ω_0 acts to increase the effect of the phonon potential energy term \hat{P}^2 in \hat{H} , thereby straightening the auxiliary field in imaginary time.

Here we have shown that the behavior of the average sign $\langle S \rangle$ in DQMC simulations holds information concerning finite density thermodynamic phases and transitions between them: the quantum critical points in the semimetal to antiferromagnetic Mott insulator transition of Dirac fermions, the band insulator to metal to correlated insulator evolution of the ionic Hubbard Hamiltonian, and the QCP of spinless fermions (even though a sign-problem free formulation exists). Specifically, a rapid evolution of $\langle S \rangle$ marks the positions of quantum critical points. We have chosen these models as representative examples of QCP physics of itinerant electrons which have been extensively studied in the condensed matter physics community, but believe the result

to be general. In fact, in a model for frustrated spins in a ladder, using a completely different QMC method (stochastic series expansion), similar conclusions can be inferred [61], further corroborating this generality.

Likewise, in the square lattice version of the $U(1)$ Hubbard model that we studied here, with an added π -flux, it can be shown that in the sign-problem free formulation, the QMC weights, when expressed in terms of the square of Pfaffians (Pf), holds similar information, namely, that $\langle \text{sgn}(\text{Pf}) \rangle$ departs from 1 close to the QCP for this model [62]. These results provide further evidence that the average sign of the QMC weights is inherently connected to the physics of the model in many unrelated models and methods, but an even broader study may be necessary to establish this conclusively.

Having established this connection in Hamiltonians with known physics, we have also presented a careful study of the sign problem for the Hubbard model on a 2D square lattice, which is of central interest to cuprate d -wave superconductivity. The intriguing ‘coincidence’ that the sign problem is worst at a density $\rho \sim 0.87$, which corresponds to the highest values of the superconducting transition temperature, has previously been noted [32, 57–59]. It is worth emphasizing that we have not here presented any *solution* to the sign problem. However, our work does establish the surprising fact that $\langle \mathcal{S} \rangle$ can be used as an ‘observable’ which can quite accurately locate quantum critical points in models like the spinful and spinless Hubbard Hamiltonians on a honeycomb lattice, and the ionic Hubbard model, and also provides a clearer connection between the evolution of the fermion sign and the strange metal/pseudogap and superconducting phases of the iconic square lattice Hubbard model.

Acknowledgments We acknowledge insightful discussions with S.-J. Hu and H.-Q. Lin. **Funding:** R.T.S. was supported by the grant DE-SC0014671 funded by the U.S. Department of Energy, Office of Science. R.M. acknowledges support from the National Natural Science Foundation of China (NSFC) Grants No. NSAF-U1930402, No. 11974039 and No. 12050410263. Computations were performed on the Tianhe-2JK at the Beijing Computational Science Research Center. **Author contributions:** R.T.S proposed the original idea for the honeycomb lattice; R.M. suggested its extension to the ionic and spinless fermion cases. All authors considered the square lattice Hubbard model, performed numerical simulations, analyzed data, and co-wrote the manuscript. **Competing interests:** Authors declare no competing interests. **Data and materials availability:** All data needed to evaluate the conclusions in the paper are presented in the main text or the supplementary materials. Further raw data is available at [63].

* rmondaini@csrc.ac.cn

† tarats@csrc.ac.cn

‡ scalett@physics.ucdavis.edu

- [1] B. Hammond, W. Lester, and P. Reynolds, *Monte Carlo Methods in Ab Initio Quantum Chemistry*, Lecture and Course Notes in Chemistry: Volume 1 (World Scientific, 1994).
- [2] R. Needs, M. Towler, N. Drummond, P. López Ríos, and J. Trail, Variational and diffusion quantum Monte Carlo calculations with the CASINO code, *J. Chem. Phys.* **152**, 154106 (2020).
- [3] D. Ceperley, Path integrals in the theory of condensed Helium, *Rev. Mod. Phys.* **67**, 279 (1995).
- [4] W. Foulkes, L. Mitas, R. Needs, and G. Rajagopal, Quantum Monte Carlo simulations of solids, *Rev. Mod. Phys.* **73**, 33 (2001).
- [5] J. Carlson, S. Gandolfi, F. Pederiva, S. C. Pieper, R. Schiavilla, K. Schmidt, and R. Wiringa, Quantum Monte Carlo methods for nuclear physics, *Rev. Mod. Phys.* **87**, 1067 (2015).
- [6] T. Degrand and C. DeTar, *Lattice Methods for Quantum Chromodynamics* (World Scientific, 2006).
- [7] See Supplemental Material, and references therein, for a review of the sign problem, more details of different observables, and further analysis of the average sign.
- [8] T. Esslinger, Fermi-Hubbard physics with atoms in an optical lattice, *Annu. Rev. Condens. Matter Phys.* **1**, 129 (2010).
- [9] I. Bloch, J. Dalibard, and S. Nascimbène, Quantum simulations with ultracold quantum gases, *Nat. Phys.* **8**, 267 (2012).
- [10] F. Schäfer, T. Fukuhara, S. Sugawa, Y. Takasu, and Y. Takahashi, Tools for quantum simulation with ultracold atoms in optical lattices, *Nat. Rev. Phys.* **2**, 411 (2020).
- [11] J. Preskill, Quantum computing in the NISQ era and beyond, *Quantum* **2**, 79 (2018).
- [12] G. Clemente, M. Cardinali, C. Bonati, E. Calore, L. Cosmai, M. D’Elia, A. Gabbana, D. Rossini, F. S. Schifano, R. Tripiccion, and D. Vadacchino (QuBiPF Collaboration), Quantum computation of thermal averages in the presence of a sign problem, *Phys. Rev. D* **101**, 074510 (2020).
- [13] M. Troyer and U.-J. Wiese, Computational complexity and fundamental limitations to fermionic quantum Monte Carlo simulations, *Phys. Rev. Lett.* **94**, 170201 (2005).
- [14] D. Hangleiter, I. Roth, D. Nagaj, and J. Eisert, Easing the monte carlo sign problem, *Science Advances* **6**, 10.1126/sciadv.abb8341 (2020).
- [15] Z.-Q. Wan, S.-X. Zhang, and H. Yao, Mitigating sign problem by automatic differentiation (2020), [arXiv:2010.01141 \[cond-mat.str-el\]](https://arxiv.org/abs/2010.01141).
- [16] Z. Meng, S. Wessel, A. Muramatsu, T. Lang, and F. Asaad, Quantum spin liquid emerging in two-dimensional correlated Dirac fermions, *Nature* **464**, 847 (2010).
- [17] S. Sorella, Y. Otsuka, and S. Yunoki, Absence of a spin liquid phase in the Hubbard model on the honeycomb lattice, *Sci. Rep.* **2**, 992 (2012).
- [18] M. Fabrizio, A. O. Gogolin, and A. A. Nersisyan, From band insulator to Mott insulator in one dimension,

- Phys. Rev. Lett.* **83**, 2014 (1999).
- [19] L. Craco, P. Lombardo, R. Hayn, G. Japaridze, and E. Müller-Hartmann, Electronic phase transitions in the half-filled ionic Hubbard model, *Phys. Rev. B* **78**, 075121 (2008).
- [20] A. Garg, H. Krishnamurthy, and M. Randeria, Doping a correlated band insulator: A new route to half-metallic behavior, *Phys. Rev. Lett.* **112**, 106406 (2014).
- [21] E. F. Huffman and S. Chandrasekharan, Solution to sign problems in half-filled spin-polarized electronic systems, *Phys. Rev. B* **89**, 111101 (2014).
- [22] L. Wang, P. Corboz, and M. Troyer, Fermionic quantum critical point of spinless fermions on a honeycomb lattice, *New J. Phys.* **16**, 103008 (2014).
- [23] B. Keimer, S. A. Kivelson, M. R. Norman, S. Uchida, and J. Zaanen, From quantum matter to high-temperature superconductivity in copper oxides, *Nature* **518**, 179 (2015).
- [24] J. Hirsch, R. Sugar, D. Scalapino, and R. Blankenbecler, Monte Carlo simulations of one-dimensional fermion systems, *Phys. Rev. B* **26**, 5033 (1982).
- [25] D. Ceperley and B. Alder, Quantum Monte Carlo for molecules: Green's function and nodal release, *J. Chem. Phys.* **81**, 5833 (1984).
- [26] M. A. Lee and K. E. Schmidt, Green's function Monte Carlo, *Comput. Phys.* **6**, 192 (1992).
- [27] P. Henelius and A. W. Sandvik, Sign problem in Monte Carlo simulations of frustrated quantum spin systems, *Phys. Rev. B* **62**, 1102 (2000).
- [28] R. Blankenbecler, D. Scalapino, and R. Sugar, Monte Carlo calculations of coupled boson-fermion systems. I, *Phys. Rev. D* **24**, 2278 (1981).
- [29] S. White, D. Scalapino, R. Sugar, E. Loh, J. Gubernatis, and R. Scalettar, Numerical study of the two-dimensional Hubbard model, *Phys. Rev. B* **40**, 506 (1989).
- [30] S. Zhang, J. Carlson, and J. E. Gubernatis, Constrained path Monte Carlo method for fermion ground states, *Phys. Rev. B* **55**, 7464 (1997).
- [31] M. Iazzi, A. A. Soluyanov, and M. Troyer, Topological origin of the fermion sign problem, *Phys. Rev. B* **93**, 115102 (2016).
- [32] E. Loh, J. Gubernatis, R. Scalettar, S. White, D. Scalapino, and R. Sugar, Sign problem in the numerical simulation of many-electron systems, *Phys. Rev. B* **41**, 9301 (1990).
- [33] C. Wu and S.-C. Zhang, Sufficient condition for absence of the sign problem in the fermionic quantum Monte Carlo algorithm, *Phys. Rev. B* **71**, 155115 (2005).
- [34] Z.-X. Li, Y.-F. Jiang, and H. Yao, Majorana-time-reversal symmetries: A fundamental principle for sign-problem-free quantum Monte Carlo simulations, *Phys. Rev. Lett.* **117**, 267002 (2016).
- [35] S. Chandrasekharan, Fermion bag approach to lattice field theories, *Phys. Rev. D* **82**, 025007 (2010).
- [36] E. Berg, M. A. Metlitski, and S. Sachdev, Sign-problem-free quantum Monte Carlo of the onset of antiferromagnetism in metals, *Science* **338**, 1606 (2012).
- [37] L. Wang, Y.-H. Liu, M. Iazzi, M. Troyer, and G. Harcos, Split orthogonal group: A guiding principle for sign-problem-free fermionic simulations, *Phys. Rev. Lett.* **115**, 250601 (2015).
- [38] Z.-X. Li and H. Yao, Sign-problem-free fermionic quantum Monte Carlo: Developments and applications, *Annu. Rev. Condens. Matter Phys.* **10**, 337 (2019).
- [39] This is just a rough guideline; the precise onset of the SP is determined by lattice geometry, doping (chemical potential), and interaction strength. A catalog of the SP in DQMC for the single band Hubbard model in different situations is given in Ref. [59].
- [40] J. Hirsch, Discrete Hubbard-Stratonovich transformation for fermion lattice models, *Phys. Rev. B* **28**, 4059 (1983).
- [41] Z.-X. Li, Y.-F. Jiang, and H. Yao, Solving the fermion sign problem in quantum Monte Carlo simulations by Majorana representation, *Phys. Rev. B* **91**, 241117 (2015).
- [42] T. Paiva, R. Scalettar, W. Zheng, R. Singh, and J. Oitmaa, Ground-state and finite-temperature signatures of quantum phase transitions in the half-filled Hubbard model on a honeycomb lattice, *Phys. Rev. B* **72**, 085123 (2005).
- [43] H. Rieger and A. P. Young, Zero-temperature quantum phase transition of a two-dimensional Ising spin glass, *Phys. Rev. Lett.* **72**, 4141 (1994).
- [44] A. Kampf, M. Sekania, G. Japaridze, and P. Brune, Nature of the insulating phases in the half-filled ionic Hubbard model, *Journal of Physics: Condensed Matter* **15**, 5895 (2003).
- [45] A. Garg, H. Krishnamurthy, and M. Randeria, Can correlations drive a band insulator metallic?, *Phys. Rev. Lett.* **97**, 046403 (2006).
- [46] N. Paris, K. Bouadim, F. Hebert, G. Batrouni, and R. Scalettar, Quantum Monte Carlo study of an interaction-driven band-insulator-to-metal transition, *Phys. Rev. Lett.* **98**, 046403 (2007).
- [47] A. Chattopadhyay, S. Bag, H. R. Krishnamurthy, and A. Garg, Phase diagram of the half-filled ionic Hubbard model in the limit of strong correlations, *Phys. Rev. B* **99**, 155127 (2019).
- [48] S. Hesselmann and S. Wessel, Thermal Ising transitions in the vicinity of two-dimensional quantum critical points, *Phys. Rev. B* **93**, 155157 (2016).
- [49] A. Damascelli, Z. Hussain, and Z.-X. Shen, Angle-resolved photoemission studies of the cuprate superconductors, *Rev. Mod. Phys.* **75**, 473 (2003).
- [50] P. A. Lee, N. Nagaosa, and X.-G. Wen, Doping a Mott insulator: Physics of high-temperature superconductivity, *Rev. Mod. Phys.* **78**, 17 (2006).
- [51] H.-C. Jiang and T. P. Devereaux, Superconductivity in the doped Hubbard model and its interplay with next-nearest hopping t' , *Science* **365**, 1424 (2019).
- [52] E. W. Huang, R. Sheppard, B. Moritz, and T. P. Devereaux, Strange metallicity in the doped Hubbard model, *Science* **366**, 987 (2019).
- [53] M. Randeria, N. Trivedi, A. Moreo, and R. T. Scalettar, Pairing and spin gap in the normal state of short coherence length superconductors, *Phys. Rev. Lett.* **69**, 2001 (1992).
- [54] A.-M. S. Tremblay, B. Kyung, and D. Sénéchal, Pseudogap and high-temperature superconductivity from weak to strong coupling. towards a quantitative theory (review article), *Low Temperature Physics* **32**, 424 (2006).
- [55] T. A. Maier, M. Jarrell, T. C. Schulthess, P. R. C. Kent, and J. B. White, Systematic study of d -wave superconductivity in the 2d repulsive Hubbard model, *Phys. Rev. Lett.* **95**, 237001 (2005).

- [56] T. A. Maier, P. Staar, V. Mishra, U. Chatterjee, J. C. Campuzano, and D. J. Scalapino, Pairing in a dry Fermi sea, *Nat. Comm.* **7**, 11875 (2016).
- [57] S. R. White, D. J. Scalapino, R. L. Sugar, N. E. Bickers, and R. T. Scalettar, Attractive and repulsive pairing interaction vertices for the two-dimensional Hubbard model, *Phys. Rev. B* **39**, 839 (1989).
- [58] D. Scalapino, Does the Hubbard model have the right stuff?, in *Proceedings of the International School of Physics*, edited by R. Broglia and J. Schrieffer (North-Holland, 1994).
- [59] V. Iglovikov, E. Khatami, and R. Scalettar, Geometry dependence of the sign problem in quantum Monte Carlo simulations, *Phys. Rev. B* **92**, 045110 (2015).
- [60] J. Hirsch, unpublished.
- [61] S. Wessel, B. Normand, F. Mila, and A. Honecker, Efficient Quantum Monte Carlo simulations of highly frustrated magnets: the frustrated spin-1/2 ladder, *SciPost Phys.* **3**, 005 (2017).
- [62] A. Goetz, S. Beyl, M. Hohenadler, and F. F. Assaad, Langevin dynamics simulations of the two-dimensional Su-Schrieffer-Heeger model (2021), [arXiv:2102.08899 \[cond-mat.str-el\]](https://arxiv.org/abs/2102.08899).
- [63] R. Mondaini, S. Tarat, and R. T. Scalettar, [Datasets to produce figures of the manuscript “Quantum Critical Points and the Sign Problem”](#) (2021).
- [64] H. A. Bethe and E. E. Salpeter, *Quantum Mechanics of One- and Two-Electron Atoms* (Springer-Verlag, 1957).
- [65] J. B. Anderson, A random-walk simulation of the Schrödinger equation: H+3, *J. Chem. Phys.* **63**, 1499 (1975).
- [66] D. Ceperley and B. Alder, Ground state of the electron gas by a stochastic method, *Phys. Rev. Lett.* **45**, 566 (1980).
- [67] J. W. Negele, Monte carlo studies of nuclear many-particle systems, *J. Stat. Phys.* **43**, 991 (1986).
- [68] J. Lynn, I. Tews, S. Gandolfi, and A. Lovato, Quantum Monte Carlo methods in nuclear physics: Recent advances, *Annu. Rev. Nucl. Part. Sci.* **69**, 279 (2019).
- [69] J. B. Kogut, An introduction to lattice gauge theory and spin systems, *Rev. Mod. Phys.* **51**, 659 (1979).
- [70] J. B. Kogut, The lattice gauge theory approach to quantum chromodynamics, *Rev. Mod. Phys.* **55**, 775 (1983).
- [71] G. Sugiyama and S. E. Koonin, Auxiliary field Monte-Carlo for quantum many-body ground states, *Ann. Phys.* **168**, 1 (1986).
- [72] G. G. Batrouni, G. R. Katz, A. S. Kronfeld, G. P. Lepage, B. Svetitsky, and K. G. Wilson, Langevin simulations of lattice field theories, *Phys. Rev. D* **32**, 2736 (1985).
- [73] S. Duane and J. B. Kogut, Hybrid stochastic differential equations applied to quantum chromodynamics, *Phys. Rev. Lett.* **55**, 2774 (1985).
- [74] S. Gottlieb, W. Liu, D. Toussaint, R. L. Renken, and R. L. Sugar, Hybrid-molecular-dynamics algorithms for the numerical simulation of quantum chromodynamics, *Phys. Rev. D* **35**, 2531 (1987).
- [75] R. T. Scalettar, D. J. Scalapino, and R. L. Sugar, New algorithm for the numerical simulation of fermions, *Phys. Rev. B* **34**, 7911 (1986).
- [76] R. T. Scalettar, D. J. Scalapino, R. L. Sugar, and D. Toussaint, Hybrid molecular-dynamics algorithm for the numerical simulation of many-electron systems, *Phys. Rev. B* **36**, 8632 (1987).
- [77] C. T. H. Davies, G. G. Batrouni, G. R. Katz, A. S. Kronfeld, G. P. Lepage, K. G. Wilson, P. Rossi, and B. Svetitsky, Fourier acceleration in lattice gauge theories. I. Landau gauge fixing, *Phys. Rev. D* **37**, 1581 (1988).
- [78] G. M. Buendia, Comparative study of the discrete and the continuous Hubbard-Stratonovich transformation for a one-dimensional spinless fermion model, *Phys. Rev. B* **33**, 3519 (1986).
- [79] L. Chen and A.-M. Tremblay, Determinant Monte Carlo for the Hubbard model with arbitrarily gauged auxiliary fields, *Int. J. Mod. Phys. B* **06**, 547 (1992).
- [80] F. F. Assaad, Quantum Monte Carlo methods on lattices: The determinantal approach, in *Quantum Simulations of Complex Many-Body Systems: From Theory to Algorithms, Lecture Notes NIC Series*, Vol. 10 (2002) pp. 99–156.
- [81] J. Gubernatis, N. Kawashima, and P. Werner, *Quantum Monte Carlo Methods: Algorithms for Lattice Models* (Cambridge University Press, 2016).
- [82] Y. Alhassid, Auxiliary-field quantum Monte Carlo methods in nuclei, in *Emergent Phenomena in Atomic Nuclei from Large-Scale Modeling: a Symmetry-Guided Perspective*, edited by K. D. Launey (World Scientific, 2017).
- [83] H. Hao, B. M. Rubenstein, and H. Shi, Auxiliary field quantum Monte Carlo for multiband Hubbard models: Controlling the sign and phase problems to capture Hund’s physics, *Phys. Rev. B* **99**, 235142 (2019).
- [84] Y.-Y. He, M. Qin, H. Shi, Z.-Y. Lu, and S. Zhang, Finite-temperature auxiliary-field quantum Monte Carlo: Self-consistent constraint and systematic approach to low temperatures, *Phys. Rev. B* **99**, 045108 (2019).
- [85] J. E. Hirsch, Two-dimensional Hubbard model: Numerical simulation study, *Phys. Rev. B* **31**, 4403 (1985).
- [86] M. Alford, A. Kapustin, and F. Wilczek, Imaginary chemical potential and finite fermion density on the lattice, *Phys. Rev. D* **59**, 054502 (1999).
- [87] J. Toulouse, R. Assaraf, and C. J. Umrigar, Introduction to the variational and diffusion Monte Carlo methods, in *Electron Correlation in Molecules – ab initio Beyond Gaussian Quantum Chemistry*, Advances in Quantum Chemistry, Vol. 73, edited by P. E. Hoggan and T. Ozdogan (Academic Press, 2016) pp. 285 – 314.
- [88] P. de Forcrand and O. Philipsen, The QCD phase diagram for small densities from imaginary chemical potential, *Nucl. Phys. B.* **642**, 290 (2002).
- [89] R. V. Gavai and S. Gupta, Pressure and nonlinear susceptibilities in QCD at finite chemical potentials, *Phys. Rev. D* **68**, 034506 (2003).
- [90] C. Allton, S. Ejiri, S. Hands, O. Kaczmarek, F. Karsch, E. Laermann, C. Schmidt, and L. Scorzato, QCD thermal phase transition in the presence of a small chemical potential, *Phys. Rev. D* **66**, 074507 (2002).
- [91] C. Adami and S. E. Koonin, Complex Langevin equation and the many-fermion problem, *Phys. Rev. C* **63**, 034319 (2001).
- [92] C. E. Berger, L. Rammelmüller, A. C. Loheac, F. Ehmman, J. Braun, and J. E. Drut, Complex Langevin and other approaches to the sign problem in quantum many-body physics (2019), [arXiv:1907.10183 \[cond-mat.quant-gas\]](https://arxiv.org/abs/1907.10183).

- [93] E. Witten, A new look at the path integral of quantum mechanics (2010), [arXiv:1009.6032 \[hep-th\]](#).
- [94] M. Cristoforetti, F. Di Renzo, and L. Scorzato (Aurora-Science Collaboration), New approach to the sign problem in quantum field theories: High density QCD on a Lefschetz thimble, *Phys. Rev. D* **86**, 074506 (2012).
- [95] M. C. Bañuls and K. Cichy, Review on novel methods for lattice gauge theories (2019), [arXiv:1910.00257 \[hep-lat\]](#).
- [96] G. Ortiz, D. Ceperley, and R. Martin, New stochastic method for systems with broken time-reversal symmetry: 2D fermions in a magnetic field, *Phys. Rev. Lett.* **71**, 2777 (1993).
- [97] S. Chandrasekharan and U.-J. Wiese, Meron-cluster solution of fermion sign problems, *Phys. Rev. Lett.* **83**, 3116 (1999).
- [98] S. Bergkvist, P. Henelius, and A. Rosengren, Reduction of the sign problem using the meron-cluster approach, *Phys. Rev. E* **68**, 016122 (2003).
- [99] M. Nyfeler, F.-J. Jiang, F. Kämpfer, and U.-J. Wiese, Nested cluster algorithm for frustrated quantum antiferromagnets, *Phys. Rev. Lett.* **100**, 247206 (2008).
- [100] Y. Nomura, S. Sakai, and R. Arita, Multiorbital cluster dynamical mean-field theory with an improved continuous-time quantum Monte Carlo algorithm, *Phys. Rev. B* **89**, 195146 (2014).
- [101] A. Mukherjee and M. Cristoforetti, Lefschetz thimble Monte Carlo for many-body theories: A Hubbard model study, *Phys. Rev. B* **90**, 035134 (2014).
- [102] H. Shinaoka, Y. Nomura, S. Biermann, M. Troyer, and P. Werner, Negative sign problem in continuous-time quantum Monte Carlo: Optimal choice of single-particle basis for impurity problems, *Phys. Rev. B* **92**, 195126 (2015).
- [103] R. K. Kaul, Marshall-positive $SU(N)$ quantum spin systems and classical loop models: A practical strategy to design sign-problem-free spin hamiltonians, *Phys. Rev. B* **91**, 054413 (2015).
- [104] M. Fukuma, N. Matsumoto, and N. Umeda, Applying the tempered Lefschetz thimble method to the Hubbard model away from half filling, *Phys. Rev. D* **100**, 114510 (2019).
- [105] M. Ulybyshev, C. Winterowd, and S. Zafeiropoulos, Lefschetz thimbles decomposition for the Hubbard model on the hexagonal lattice, *Phys. Rev. D* **101**, 014508 (2020).
- [106] A. J. Kim, P. Werner, and R. Valentí, Alleviating the sign problem in quantum Monte Carlo simulations of spin-orbit-coupled multiorbital Hubbard models, *Phys. Rev. B* **101**, 045108 (2020).
- [107] R. Wiringa, S. C. Pieper, J. Carlson, and V. Pandharipande, Quantum Monte Carlo calculations of $A = 8$ nuclei, *Phys. Rev. C* **62**, 014001 (2000).
- [108] S. Gandolfi, D. Lonardonì, A. Lovato, and M. Piarulli, Atomic nuclei from quantum Monte Carlo calculations with chiral EFT interactions, *Frontiers in Physics* **8**, 117 (2020).
- [109] C. Umrigar, J. Toulouse, C. Filippi, S. Sorella, and R. Hennig, Alleviation of the fermion-sign problem by optimization of many-body wave functions, *Phys. Rev. Lett.* **98**, 110201 (2007).
- [110] H. Shi, C. A. Jiménez-Hoyos, R. Rodríguez-Guzmán, G. E. Scuseria, and S. Zhang, Symmetry-projected wave functions in quantum Monte Carlo calculations, *Phys. Rev. B* **89**, 125129 (2014).
- [111] A. Roggero and F. Pederiva, Extension of the configuration interaction Monte Carlo method to atoms and molecules, in *Novel Electronic Structure Theory: General Innovations and Strongly Correlated Systems*, edited by P. Hoggan (Elsevier, 2018) Chap. 13, pp. 241–253.
- [112] S. Rothstein, E. Ospadov, and C. Bruzzese, Introduction to fixed-node quantum Monte Carlo, in *Mathematical Physics in Theoretical Chemistry*, edited by S. Blinder and J. House (Elsevier, 2019) Chap. 6, pp. 189–217.
- [113] I. Bloch, Ultracold quantum gases in optical lattices, *Nat. Phys.* **1**, 23 (2005).
- [114] L. Tarruell and L. Sanchez-Palencia, Quantum simulation of the hubbard model with ultracold fermions in optical lattices, *Comptes Rendus Physique* **19**, 365 (2018), quantum simulation / Simulation quantique.
- [115] G. Ortiz, J. Gubernatis, E. Knill, and R. Laflamme, Quantum algorithms for fermionic simulations, *Phys. Rev. A* **64**, 022319 (2001).
- [116] K. Brown, W. Munro, and V. Kendon, Using quantum computers for quantum simulation, *Entropy* **12**, 2268 (2010).
- [117] M. Steudtner and S. Wehner, Fermion-to-qubit mappings with varying resource requirements for quantum simulation, *New J. Phys.* **20**, 063010 (2018).
- [118] Google AI Quantum and collaborators, Observation of separated dynamics of charge and spin in the Fermi-Hubbard model (2020), [arXiv:2010.07965 \[quant-ph\]](#).
- [119] N. Kawashima and K. Harada, Recent developments of world-line Monte Carlo methods, *J. Phys. Soc. Jpn.* **73**, 1379 (2004).
- [120] P. J. Reynolds, J. Tobochnik, and H. Gould, Diffusion quantum Monte Carlo, *Comput. Phys.* **4**, 662 (1990).
- [121] A. Georges, G. Kotliar, W. Krauth, and M. J. Rozenberg, Dynamical mean-field theory of strongly correlated fermion systems and the limit of infinite dimensions, *Rev. Mod. Phys.* **68**, 13 (1996).
- [122] B. Beard and U.-J. Wiese, Simulations of discrete quantum systems in continuous Euclidean time, *Phys. Rev. Lett.* **77**, 5130 (1996).
- [123] M. Hettler, M. Mukherjee, M. Jarrell, and H. Krishnamurthy, Dynamical cluster approximation: Nonlocal dynamics of correlated electron systems, *Phys. Rev. B* **61**, 12739 (2000).
- [124] G. Kotliar, S. Y. Savrasov, G. Pálsson, and G. Biroli, Cellular dynamical mean field approach to strongly correlated systems, *Phys. Rev. Lett.* **87**, 186401 (2001).
- [125] A. Rubtsov, V. Savkin, and A. Lichtenstein, Continuous-time quantum Monte Carlo method for fermions, *Phys. Rev. B* **72**, 035122 (2005).
- [126] T. Maier, M. Jarrell, T. Pruschke, and M. H. Hettler, Quantum cluster theories, *Rev. Mod. Phys.* **77**, 1027 (2005).
- [127] B. Kyung, G. Kotliar, and A.-M. S. Tremblay, Quantum Monte Carlo study of strongly correlated electrons: Cellular dynamical mean-field theory, *Phys. Rev. B* **73**, 205106 (2006).
- [128] E. Gull, P. Werner, O. Parcollet, and M. Troyer, Continuous-time auxiliary-field Monte Carlo for quantum impurity models, *EPL (Europhysics Letters)* **82**, 57003 (2008).
- [129] E. Gull, A. J. Millis, A. I. Lichtenstein, A. N. Rubtsov, M. Troyer, and P. Werner, Continuous-time Monte

- Carlo methods for quantum impurity models, *Rev. Mod. Phys.* **83**, 349 (2011).
- [130] N. Prokofév, B. Svistunov, and I. Tupitsyn, Exact quantum Monte Carlo process for the statistics of discrete systems, *JETP Lett.* **64**, 911 (1996).
- [131] K. V. Houcke, E. Kozicka, N. Prokofév, and B. Svistunov, Diagrammatic Monte Carlo, *Physics Procedia* **6**, 95 (2010).
- [132] R. Rossi, Determinant diagrammatic Monte Carlo algorithm in the thermodynamic limit, *Phys. Rev. Lett.* **119**, 045701 (2017).
- [133] G. Rohringer, H. Hafermann, A. Toschi, A. Katanin, A. Antipov, M. Katsnelson, A. Lichtenstein, A. Rubtsov, and K. Held, Diagrammatic routes to nonlocal correlations beyond dynamical mean field theory, *Rev. Mod. Phys.* **90**, 025003 (2018).
- [134] J. E. Hirsch, Connection between world-line and determinantal functional-integral formulations of the Hubbard model, *Phys. Rev. B* **34**, 3216 (1986).
- [135] G. G. Batrouni and R. T. Scalettar, Anomalous decouplings and the fermion sign problem, *Phys. Rev. B* **42**, 2282 (1990).
- [136] A. Georges and G. Kotliar, Hubbard model in infinite dimensions, *Phys. Rev. B* **45**, 6479 (1992).
- [137] M. Jarrell, Hubbard model in infinite dimensions: A quantum Monte Carlo study, *Phys. Rev. Lett.* **69**, 168 (1992).
- [138] M. Jarrell, T. Maier, C. Huscroft, and S. Moukouri, Quantum Monte Carlo algorithm for nonlocal corrections to the dynamical mean-field approximation, *Phys. Rev. B* **64**, 195130 (2001).
- [139] M. Hohenadler, Z. Y. Meng, T. C. Lang, S. Wessel, A. Muramatsu, and F. F. Assaad, Quantum phase transitions in the Kane-Mele-Hubbard model, *Phys. Rev. B* **85**, 115132 (2012).
- [140] M. Bercx, M. Hohenadler, and F. F. Assaad, Kane-Mele-Hubbard model on the π -flux honeycomb lattice, *Phys. Rev. B* **90**, 075140 (2014).
- [141] F. Parisen Toldin, M. Hohenadler, F. F. Assaad, and I. F. Herbut, Fermionic quantum criticality in honeycomb and π -flux Hubbard models: Finite-size scaling of renormalization-group-invariant observables from quantum Monte Carlo, *Phys. Rev. B* **91**, 165108 (2015).
- [142] J. Imriška, L. Wang, and M. Troyer, First-order topological phase transition of the Haldane-Hubbard model, *Phys. Rev. B* **94**, 035109 (2016).
- [143] T. I. Vanhala, T. Siro, L. Liang, M. Troyer, A. Harju, and P. Törmä, Topological phase transitions in the repulsively interacting Haldane-Hubbard model, *Phys. Rev. Lett.* **116**, 225305 (2016).
- [144] C. Shao, E. V. Castro, S. Hu, and R. Mondaini, Interplay of local order and topology in the extended Haldane-Hubbard model, *Phys. Rev. B* **103**, 035125 (2021).
- [145] C. Huscroft and R. Scalettar, Effect of disorder on charge-density wave and superconducting order in the half-filled attractive Hubbard model, *Phys. Rev. B* **55**, 1185 (1997).
- [146] P. J. H. Denteneer, R. T. Scalettar, and N. Trivedi, Particle-hole symmetry and the effect of disorder on the Mott-Hubbard insulator, *Phys. Rev. Lett.* **87**, 146401 (2001).
- [147] P. J. H. Denteneer, R. T. Scalettar, and N. Trivedi, Conducting phase in the two-dimensional disordered Hubbard model, *Phys. Rev. Lett.* **83**, 4610 (1999).
- [148] P. J. H. Denteneer and R. T. Scalettar, Interacting electrons in a two-dimensional disordered environment: Effect of a Zeeman magnetic field, *Phys. Rev. Lett.* **90**, 246401 (2003).
- [149] S. Sorella and E. Tosatti, Semi-metal-insulator transition of the Hubbard model in the honeycomb lattice, *Europhys. Lett.* **19**, 699 (1992).
- [150] I. F. Herbut, Interactions and phase transitions on graphene's honeycomb lattice, *Phys. Rev. Lett.* **97**, 146401 (2006).
- [151] A. Giuliani and V. Mastropietro, The two-dimensional Hubbard model on the honeycomb lattice, *Commun. Math. Phys.* **293**, 301 (2009).
- [152] T. Ma, F. Hu, Z. Huang, and H.-Q. Lin, Magnetic correlation in the Hubbard model on a honeycomb lattice, *Comput. Phys. Commun.* **182**, 52 (2011), computer Physics Communications Special Edition for Conference on Computational Physics Kaohsiung, Taiwan, Dec 15-19, 2009.
- [153] B. Clark, D. Abanin, and S. Sondhi, Nature of the spin liquid state of the Hubbard model on a honeycomb lattice, *Phys. Rev. Lett.* **107**, 087204 (2011).
- [154] M. Raczkowski, R. Peters, T. T. Phùng, N. Takemori, F. F. Assaad, A. Honecker, and J. Vahedi, Hubbard model on the honeycomb lattice: From static and dynamical mean-field theories to lattice quantum Monte Carlo simulations, *Phys. Rev. B* **101**, 125103 (2020).
- [155] F. F. Assaad and I. F. Herbut, Pinning the order: The nature of quantum criticality in the Hubbard model on honeycomb lattice, *Phys. Rev. X* **3**, 031010 (2013).
- [156] K. Bouadim, N. Paris, F. Hébert, G. Batrouni, and R. Scalettar, Metallic phase in the two-dimensional ionic Hubbard model, *Phys. Rev. B* **76**, 085112 (2007).
- [157] S. Manmana, V. Meden, R. Noack, and K. Schönhammer, Quantum critical behavior of the one-dimensional ionic Hubbard model, *Phys. Rev. B* **70**, 155115 (2004).
- [158] S. Bag, A. Garg, and H. Krishnamurthy, Phase diagram of the half-filled ionic Hubbard model, *Phys. Rev. B* **91**, 235108 (2015).
- [159] R. Fye, New results on Trotter-like approximations, *Phys. Rev. B* **33**, 6271 (1986).
- [160] M. Hirayama, Y. Yamaji, T. Misawa, and M. Imada, Ab initio effective Hamiltonians for cuprate superconductors, *Phys. Rev. B* **98**, 134501 (2018).
- [161] M. Hirayama, T. Misawa, T. Ohgoe, Y. Yamaji, and M. Imada, Effective Hamiltonian for cuprate superconductors derived from multiscale ab initio scheme with level renormalization, *Phys. Rev. B* **99**, 245155 (2019).
- [162] M. Jarrell and J. Gubernatis, Bayesian inference and the analytic continuation of imaginary-time quantum Monte Carlo data, *Phys. Rep.* **269**, 133 (1996).
- [163] N. Trivedi and M. Randeria, Deviations from Fermi-liquid behavior above T_c in 2d short coherence length superconductors, *Phys. Rev. Lett.* **75**, 312 (1995).
- [164] W. Wu, M. S. Scheurer, S. Chatterjee, S. Sachdev, A. Georges, and M. Ferrero, Pseudogap and Fermi-surface topology in the two-dimensional Hubbard model, *Phys. Rev. X* **8**, 021048 (2018).
- [165] K.-S. Chen, Z. Y. Meng, T. Pruschke, J. Moreno, and M. Jarrell, Lifshitz transition in the two-dimensional Hubbard model, *Phys. Rev. B* **86**, 165136 (2012).
- [166] B. Dalla Piazza, M. Mourigal, M. Guarise, H. Berger, T. Schmitt, K. J. Zhou, M. Gironi, and H. M. Rønnow,

Unified one-band Hubbard model for magnetic and electronic spectra of the parent compounds of cuprate superconductors, *Phys. Rev. B* **85**, 100508 (2012).

Supplementary Materials: Quantum Critical Points and the Sign Problem

In these Supplementary Materials we provide some additional context and history of the sign problem. We also show the behavior of other observables across the transitions described in the main body of the paper, as well as exploring more carefully finite spatial size and Trotter effects in the evolution of $\langle \mathcal{S} \rangle$.

CONTENTS

References	7
The Role of Quantum Simulations	13
Determinant Quantum Monte Carlo	13
Physical Observables	14
Sign Problem: General Importance	15
The sign problem in other QMC algorithms	15
The sign problem in other Hamiltonians	16
More details on the Spinful Hubbard Model on a Honeycomb Lattice (main text, Sec. I)	17
More details on the Ionic Hubbard Hamiltonian (main text, Sec. II)	18
More details on Spinless Honeycomb Hubbard (main text, Sec. III)	20
More details for the homogeneous Hubbard model on the square lattice (main text, Sec. IV)	21

THE ROLE OF QUANTUM SIMULATIONS

The motivation for numerical solutions to the quantum many body problem is the intractability of analytic solutions except in limited circumstances. Indeed, the extension of the analytic solution of the single electron Hydrogen atom to two electrons is already problematic, as emphasized in the classic text of Bethe and Salpeter [64]. As a consequence, quantum simulations approaches appeared in chemistry [25, 65], condensed matter [24, 66], nuclear [67, 68], and high energy physics [28, 69, 70] almost as soon as computers became reasonably available for scientific work.

There is considerable methodological linkage in quantum simulation between these fields. For example, in the case of the DQMC method used in this work, the problem of treating the accumulation of round off errors at low temperatures was first developed in the nuclear physics community [71] before being adapted to condensed matter. Likewise, the linear scaling methods of lattice gauge theory (LGT) [72–74] were soon adapted to condensed matter physics [75, 76], albeit with only limited success owing to the extreme anisotropic (non-relativistic) nature of the condensed matter space-imaginary time lattices. Many of the algorithms, like Fourier Acceleration, which are crucial to LGT, were first implemented and tested for classical spin models [77].

DETERMINANT QUANTUM MONTE CARLO

The DQMC method is a specific type of AFQMC [28, 29, 78–84]. In DQMC, the partition function \mathcal{Z} is expressed as a path integral and the Trotter approximation is used to isolate the quartic terms,

$$\mathcal{Z} = \text{Tr} e^{-\beta \hat{H}} = \text{Tr} [e^{-\Delta\tau \hat{H}}]^{L\tau} \sim \text{Tr} [e^{-\Delta\tau \hat{H}_t} e^{-\Delta\tau \hat{H}_U}]^{L\tau}, \quad (\text{S1})$$

where \hat{H}_t includes the hopping and chemical potential (together with all other bilinear terms in the fermionic operators), and \hat{H}_U the on-site interactions, in the Hubbard Hamiltonian of Eq. (1). The latter are then decomposed via,

$$e^{-\Delta\tau U(n_{i\uparrow}-\frac{1}{2})(n_{i\downarrow}-\frac{1}{2})} = \frac{1}{2}e^{-U\Delta\tau/4} \sum_{s_i=\pm 1} e^{\lambda s_i(n_{i\uparrow}-n_{i\downarrow})}, \quad (\text{S2})$$

where $\cosh \lambda = e^{U\Delta\tau/2}$. A Hubbard-Stratonovich variable (bosonic field) s_i must be introduced at each spatial site i and for each imaginary time slice $U_{\Delta\tau}$. The prefactor $\frac{1}{2}e^{-U\Delta\tau/4}$ is an irrelevant constant which may be dropped.

The key observation is that the right hand side of Eq. (S2) is now quadratic in the fermions, so that the partition function \mathcal{Z} is a trace over a product of quadratic forms of fermionic operators:

$$\mathcal{Z} = \sum_{\{s_{i\tau}\}} \text{Tr}_{\uparrow} [e^{\vec{c}_{\uparrow}^{\dagger} K \vec{c}_{\uparrow}} e^{\vec{c}_{\uparrow}^{\dagger} P^1 \vec{c}_{\uparrow}} \dots e^{\vec{c}_{\uparrow}^{\dagger} K \vec{c}_{\uparrow}} e^{\vec{c}_{\uparrow}^{\dagger} P^L \vec{c}_{\uparrow}}] \text{Tr}_{\downarrow} [e^{\vec{c}_{\downarrow}^{\dagger} K \vec{c}_{\downarrow}} e^{-\vec{c}_{\downarrow}^{\dagger} P^1 \vec{c}_{\downarrow}} \dots e^{\vec{c}_{\downarrow}^{\dagger} K \vec{c}_{\downarrow}} e^{-\vec{c}_{\downarrow}^{\dagger} P^L \vec{c}_{\downarrow}}], \quad (\text{S3})$$

with $\vec{c}_{\sigma}^{\dagger} = (c_{\sigma 1}^{\dagger} c_{\sigma 2}^{\dagger} \dots c_{\sigma N}^{\dagger})^T$. The matrix K is the same for all time slices and contains $\mu\Delta\tau$ along its diagonal and $t\Delta\tau$ for sites connected by the hopping. (In the case of the ionic Hubbard model, the staggered site energy term also appears along the diagonal.) The matrices P^{τ} are diagonal, with $P_{ii}^{\tau} = \lambda\sigma s_{i\tau}$ ($\sigma = \pm 1$ for \uparrow and \downarrow). All matrices have dimension equal to the number of spatial lattice sites N .

The trace of a quadratic form such as Eq. (S3) can be done analytically [28, 29, 79–84], resulting in

$$\mathcal{Z} = \sum_{\{s_{i\tau}\}} \det[I + e^K e^{P^1} \dots e^K e^{P^L}] \det[I + e^K e^{-P^1} \dots e^K e^{-P^L}]. \quad (\text{S4})$$

The expression for \mathcal{Z} of Eq. (S4) contains no quantum operators, just the matrices $K, \{P^{\tau}\}$ of the quadratic forms. Its calculation is thereby reduced to a classical Monte Carlo problem in which the sum over $\{s_{i\tau}\}$ must be done stochastically with a weight equal to the product of the two determinants. That these might become negative is the origin of the SP in DQMC.

Besides this spinful case, we have also investigated interacting spinless fermions. The problem formulation in QMC simulations is almost identical to that of the spinful case, but now the decoupling of the interactions V on each nearest-neighbor bond $\langle i, j \rangle$ reads

$$e^{-\Delta\tau V(n_i-\frac{1}{2})(n_j-\frac{1}{2})} = \frac{1}{2}e^{-V\Delta\tau/4} \sum_{s_{ij}=\pm 1} e^{\lambda s_{ij}(n_i-n_j)}, \quad (\text{S5})$$

where $\cosh \lambda = e^{V\Delta\tau/2}$. The Hubbard-Stratonovich variable s now lives on the bonds, and its total number for the rhombus-shaped space-time lattices used here is $3L^2L_{\tau}$. After a similar procedure for tracing out the fermions, one ends up with

$$\mathcal{Z} = \sum_{\{s_{ij,\tau}\}} \det[I + e^K e^{P^1} \dots e^K e^{P^L}], \quad (\text{S6})$$

where the elements of the diagonal matrix P^{τ} are $P_{ii}^{\tau} = (-1)^i \lambda \sum_j s_{ij,\tau}$. A major difference from the spinful case is that the protection that the sign of the determinants of the matrices for up and down spin channels display in bipartite lattices by getting locked together [31, 85] is no longer present. This can generically give rise to an even more detrimental SP, yet it allows us to systematically locate the QCP of Eq. (2) with a large accuracy.

PHYSICAL OBSERVABLES

The central object in the QMC simulations is the Green's function G^{σ} whose matrix elements are $G_{ij}^{\sigma}(\tau', \tau) = \langle c_{i\sigma}(\tau') c_{j\sigma}^{\dagger}(\tau) \rangle$. By using Wick contractions and the fermionic anti-commutation relations one can define all quantities used in the main text. These are the double occupancy,

$$\langle n_{\uparrow\downarrow} \rangle = \langle n_{\uparrow} n_{\downarrow} \rangle, \quad (\text{S7})$$

the static susceptibility

$$\chi(\mathbf{q}) = \frac{\beta}{N} \sum_{i,j} e^{i\mathbf{q}\cdot(\mathbf{R}_i - \mathbf{R}_j)} \langle (n_{i,\uparrow} - n_{i,\downarrow})(n_{j,\uparrow} - n_{j,\downarrow}) \rangle, \quad (\text{S8})$$

and the pair-susceptibility

$$P_\alpha = \int_0^\beta d\tau \langle \Delta_\alpha(\tau) \Delta_\alpha^\dagger(0) \rangle, \quad (\text{S9})$$

with the momentum-dependent pair operator given by

$$\Delta_\alpha^\dagger = \frac{1}{N} \sum_{\mathbf{k}} f_\alpha(\mathbf{k}) c_{\mathbf{k}\uparrow}^\dagger c_{-\mathbf{k}\downarrow}^\dagger. \quad (\text{S10})$$

The form factors $f_\alpha(\mathbf{k})$ describe the various symmetry channels investigated:

$$f_d(\mathbf{k}) = \cos k_x - \cos k_y; \quad f_{s^*}(\mathbf{k}) = \cos k_x + \cos k_y; \quad f_s(\mathbf{k}) = 1, \quad (\text{S11})$$

for d -wave, extended s -wave, and s -wave pairings, respectively. In all data presented, we subtract the uncorrelated (non-vertex) contribution, P_α^{nv} , in which pairs of fermionic operators are first averaged before taking the product, i.e., terms in Eq. (S9) such as $\langle c_{i\downarrow}^\dagger(\tau) c_{j\downarrow}(0) c_{i\downarrow}^\dagger(\tau) c_{m\downarrow}(0) \rangle$ get replaced by their decoupled contributions $\langle c_{i\downarrow}^\dagger(\tau) c_{j\downarrow}(0) \rangle \langle c_{i\downarrow}^\dagger(\tau) c_{m\downarrow}(0) \rangle$.

Other quantities used exclusively in this supplemental material are introduced in the corresponding sections.

SIGN PROBLEM: GENERAL IMPORTANCE

In lattice gauge theory, the SP is triggered by a non-zero chemical potential μ . Attempts to solve, or reduce, the SP include analytic continuation from complex to real chemical potentials μ [86, 87], Taylor expansion about zero μ [88, 89], re-weighting approaches [90], complex Langevin methods [91, 92], and Lefshetz thimble techniques [93, 94]. For a review of the SP in LGT, see Ref. [95]. A similar litany of papers, ideas, and new methods characterizing, ameliorating, or solving the SP can be found in the condensed matter [13, 27, 30, 32, 59, 84, 96–106], nuclear physics [68, 82, 107, 108], and quantum chemistry [109–112] communities. These approaches differ in detail, depending on whether they are addressing the SP in real space versus lattice models, quantum spin versus itinerant fermion, etc.

One of the dominant themes in atomic and molecular (AMO) physics over the last decade has been the possibility that ultracold atoms in an optical lattice might serve as emulators of fundamental models of condensed matter physics [8–10, 113, 114]. The initial motivation was the possibility that simplified model Hamiltonians could be more precisely realized in the AMO context than in the solid state, where materials ‘complications’ are unavoidable and often significant, if not dominant. However, it was quickly understood that an equally important advantage was that, because of the SP, the solution of these simplified models was possible only at temperatures which were well above those needed to access phenomena like d -wave superconductivity. Thus it is fair to say that the SP has been a significant driver of the enormous efforts and progress in this domain of AMO physics.

A similar theme is present in quantum computing [11, 12, 115, 116], which promises the general possibility of solving problems much more rapidly (‘quantum supremacy’) than with a classical computer. The exponential scaling time of solutions of model Hamiltonians in the presence of the SP offers one of the most significant targets for such endeavors [117, 118].

THE SIGN PROBLEM IN OTHER QMC ALGORITHMS

In exploring the linkage between the SP and critical properties, we have focused exclusively on DQMC. As noted in the previous discussion, the SP occurs also in a plethora of QMC methods: world-line quantum Monte Carlo (WLQMC) [119], Greens Function (Diffusion) Monte Carlo (GFMC) [120], in dynamical mean field theory (DMFT) and its cluster extensions (including continuous time approaches) [121–129], and in diagrammatic QMC [130–133]. It would be interesting to explore these situations as well, checking the direct correlation between the SP and regimes

of quantum critical behavior. Regarding WLQMC, it is known that the onset of the sign problem is at much higher temperature than in DQMC, and occurs due to particle exchange in the world-lines. Indeed, this provides one of the earliest examples of the dependence of the sign problem on the algorithm used. It seems probable that the restriction of WLQMC to only very high temperatures ($T/W \gtrsim 1/5$ is quite typical) might preclude the possibility of an association of the sign problem with interesting low temperature correlations and transitions. It is worth noticing that an attempt to reconcile WLQMC and DQMC was put forward by introducing more generic Hubbard-Stratonovich transformations [134]; it has been further argued that the SP in WLQMC has two origins: one from the fact that Slater determinants are anti-symmetric sums of world-line configurations and another intrinsic, akin to the one in DQMC, that has been claimed having topological origin [31]. In the same way, alternative choices of Hubbard-Stratonovich transformations in DQMC [79, 135] significantly worsen the sign problem. DMFT [121, 136, 137], on the other hand, is at the opposite end of the spectrum, with a sign problem which is greatly reduced relative to that of DQMC. Unfortunately, its cluster extensions, using QMC as the cluster solver, exhibit an increasingly serious SP at low enough temperatures as the number of points in the momentum grid increases [126, 127, 138].

We finish by noting that while we have argued that when a QCP is present, the SP provides quantitative information about its location, the converse is *not* necessarily true: a SP can exist even in the absence of a QCP. In particular, in WLQMC, free fermions have a SP in $D > 1$ without possessing any sort of phase transition. As noted above, DQMC is SP free when the interactions vanish, so this simple counter-example is not present in that algorithm.

THE SIGN PROBLEM IN OTHER HAMILTONIANS

In our work, the spinless fermion Hamiltonian on a honeycomb lattice offered a particularly concrete case where a sign problem free approach allows a detailed study of quantum critical behavior. We exploited this as a way to make a very quantitative test of the connection of the SP to the location of the QCP. In addition to exploring other algorithms, a promising further line of inquiry is to turn on a chemical potential in other ‘sign problem free’ models [34–

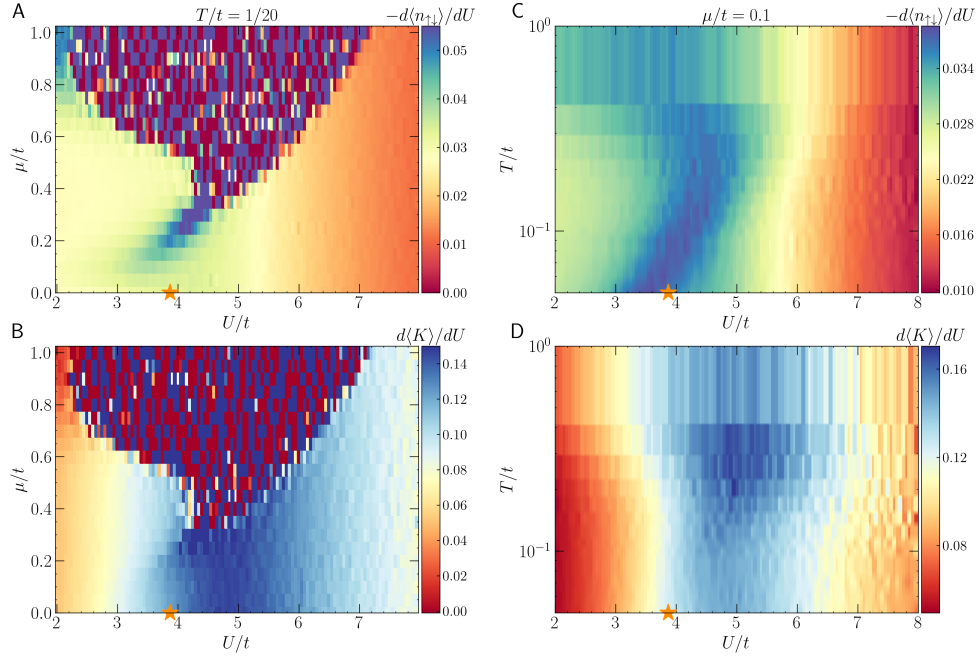


Figure S1. **Local observables in the vicinity of the quantum critical point on the SU(2) honeycomb Hubbard model.** The derivative of the double occupancy (A) and the kinetic energy (B) at $T/t = 1/20$ when approaching the quantum critical point at $\mu \rightarrow 0$ and $U_c \simeq 3.85t$. As in the main text for other models, the noisy data at large chemical potentials denotes the regime of small $\langle S \rangle$ with a vanishing signal-to-noise ratio. (C) and (D) display the same quantities when approaching $T/t \rightarrow 0$, with a small chemical potential $\mu/t = 0.1$. As in the $T = 0$ results of Ref. [16], the derivative of the kinetic energy displays a peak within the AFMI phase. Our data show this persists to finite temperatures. The lattice size used is $L = 9$, and all data are averaged among 20 independent runs.

38]. The Kane-Mele-Hubbard model would be especially interesting since it presents a framework to understand the transition from topological phases (quantum spin Hall insulator) towards a (topologically trivial) Mott insulator with antiferromagnetic order [139–141]. The Hubbard-Stratonovich transformation is slightly more complicated, and in fact a ‘phase problem’ appears instead. In exploring this competition between ordered and topological phases, the study of the Haldane-Hubbard model presents as a challenging case, since due to the absence of time-reversal symmetry, it gives rise to a severe SP in the simulations [142]. Whether similar analysis as conducted here can help in locating the QCP associated to a topological transition in system sizes exceeding the ones amenable to ED [143, 144] is yet an open question left for future studies.

A further possibility for future work includes situations where disorder drives a quantum phase transition [145]. This is of particular interest because different types of disorder can either possess particle-hole symmetry or not [146], and this dichotomy is known to be linked both to the presence of the sign problem as well as to the occurrence of metal to insulator transitions [147, 148]. Thus disordered systems might provide an especially rich arena to explore the connection between the SP and the underlying physics of the Hamiltonian.

MORE DETAILS ON THE SPINFUL HUBBARD MODEL ON A HONEYCOMB LATTICE (MAIN TEXT, SEC. I)

Energy and Double Occupation.— The quantum critical point separating the paramagnetic semimetal and the antiferromagnetic insulator (AFMI) phases of the honeycomb Hubbard hamiltonian has been characterized using observables ranging from the magnetic structure factor to the conductivity. In the main text, we focused on using the average sign as a signal of the QCP. Here we provide context by showing some of the traditional measurements. More detailed results are contained in the literature [16, 17, 42, 149–154].

Figure S1 shows the derivatives of the average kinetic energy $\langle K \rangle = \frac{-t}{2L^2} \sum_{\langle i,j \rangle, \sigma} (c_{i\sigma}^\dagger c_{j\sigma} + c_{j\sigma}^\dagger c_{i\sigma})$ and double occupation $\langle n_{\uparrow\downarrow} \rangle$ with respect to U across the honeycomb lattice transition from semimetal to AFMI. Both show clear signals in the vicinity of U_c . The accurate indication of antiferromagnetic long range order requires a careful finite size scaling analysis of the antiferromagnetic structure factor, which can be found in Refs. [16, 17, 42].

Individual spin channel average sign in the Spinful Hubbard Model on a Honeycomb Lattice.— In the main text, we have demonstrated how the average sign can be used as a ‘tracker’ of quantum critical behavior. In the case of models within regimes where a sign problem is absent, e.g., for an SU(2) Hubbard model on a bipartite lattice, this ability is no longer available if the chemical potential $\mu = 0$, since the determinants of the two spin species always

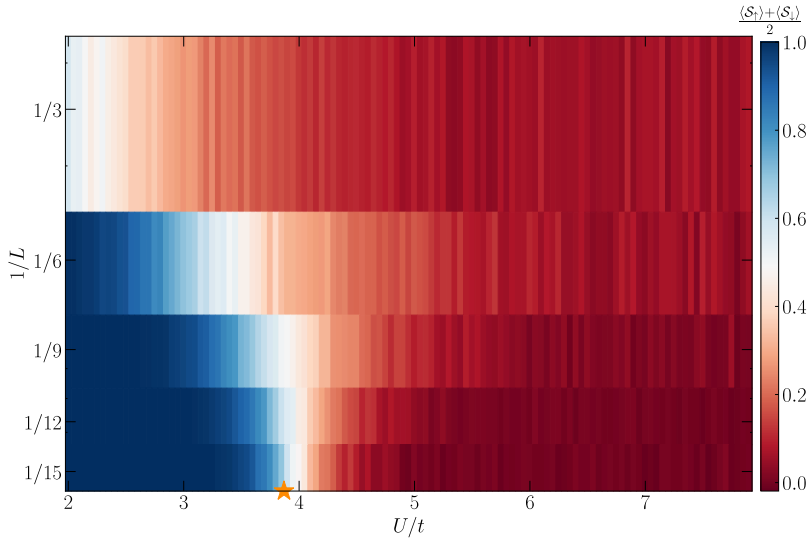


Figure S2. **Spin resolved sign for the SU(2) Hubbard model on the honeycomb lattice.** The scaling with the inverse of the linear system size L of the average sign of individual determinants in the case there is no sign problem: $\mu/t = 0$. The star marker depicts the best known estimation of the critical value $U_c/t = 3.869$ [17] at the ground state for the onset of the Mott insulating phase with AFM order. All data are extracted at $T/t = 1/20$, with $\Delta\tau = 0.1$.

have the same sign so that their product is positive. This can be proven by considering a staggered particle-hole transformation (PHT) $c_{i\downarrow}^\dagger \rightarrow (-1)^i c_{i\downarrow}$ on the down spin species. Here $(-1)^i = +1(-1)$ on sublattice A(B). Under the PHT, the kinetic energy matrix K of Eqs. (S3),(S4) remains invariant, but the matrices P^τ in the down spin trace change sign, making the down spin determinant the same as the up spin determinant, up to a positive factor $e^{\lambda \sum_{i\tau} s_{i\tau}}$ [85].

While the *product* of the determinants is always positive in this situation, the QCP remains imprinted in the average sign of the determinants for *individual* spin components $\langle \mathcal{S}_\sigma \rangle$. To illustrate this, we consider the first model used in the main text, the repulsive spinful Hubbard model on the (bipartite) honeycomb lattice. Figure S2 plots $\langle \mathcal{S}_\sigma \rangle$ ($\sigma = \uparrow, \downarrow$) at fixed $T/t = 1/20$. The individual signs are largely positive in the metallic phase, but rather abruptly change to equally positive and negative ($\langle \mathcal{S} \rangle \sim 0$) in the AFMI phase $U > U_c$. The match of the transition in the sign and the position of the QCP becomes increasingly precise in the thermodynamic limit $1/L \rightarrow 0$. The sharpness of the drop in $\langle \mathcal{S}_\sigma \rangle$ with increasing system sizes is suggestive of a possible scaling form for this quantity. Preliminary data, to be presented elsewhere, indicates a scaling with critical exponents compatible with the ones obtained from physical observables [155].

MORE DETAILS ON THE IONIC HUBBARD HAMILTONIAN (MAIN TEXT, SEC. II)

Finite-size effects.— The ionic Hubbard model presents a unique situation in our study: instead of displaying a quantum critical point at half-filling, it exhibits a quantum critical regime, associated with a correlated metal (CM) phase [18–20, 44–46, 156–158]. We argued in the main text that this phase, sandwiched between the band-insulator (BI) at large Δ , and the Mott insulator (MI) at large U , can be indicated by a vanishing average sign in the DQMC simulations. We now explore the influence of finite-size effects on those phase boundaries, for a specific value of the staggered potential $\Delta/t = 0.5$.

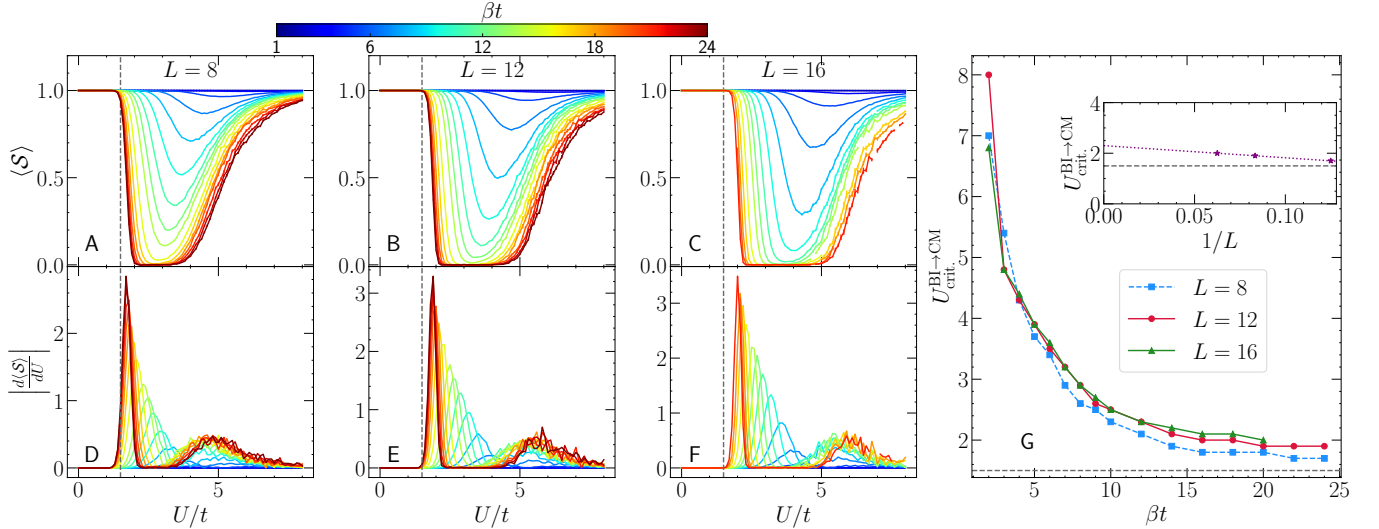


Figure S3. **Finite-size analysis: Ionic Hubbard model.** (A, B, C) The average sign $\langle \mathcal{S} \rangle$ for decreasing temperatures (growing $\beta = 1/T$) as a function of the Hubbard interaction U/t in a lattice with $L = 8, 12$ and 16 with a staggered potential $\Delta/t = 0.5$. (D, E, F) The corresponding magnitude of the derivative of $\langle \mathcal{S} \rangle$ in respect to U at each lattice size. (G) Peak position of the derivative of the average sign with different inverse temperatures β ; the inset presents an extrapolation to the thermodynamic limit of the estimated transition from the BI to the CM phase, as inferred by the first peak of $|d\langle \mathcal{S} \rangle/dU|$. The gray dashed lines in all panels display the corresponding transition value obtained in Ref. [156]. All data are averaged over 24 independent runs, with $\Delta\tau = 0.1$.

Figure S3 indicates that the first transition which occurs upon increasing U/t from zero, that from BI to CM, is well marked by a fast drop of $\langle \mathcal{S} \rangle$ at lower temperatures. A quantitative estimation of the transition point can be extracted by differentiating the average sign with respect to the interaction strength, $d\langle \mathcal{S} \rangle/dU$ (lower panels in Fig. S3). As the temperature is lowered, the peak position quickly approaches the best known values of the transition for this set of parameters [156], see Fig. S3(G). The system size dependence is reasonably small. The second transition, from CM

to AFI, on the other hand, displays characteristics reminiscent of a crossover for the system sizes and temperatures investigated. The estimate given by the peak of the average sign also displays a stronger dependence on L , and, overall, is larger than the value of the position of the metal-AF transition at this Δ obtained in Ref. [156]. It is worth mentioning that these values in the existing literature were extracted at smaller lattice sizes than the largest L used here. A finite size extrapolation of the ‘traditional’ correlations used to obtain U_c for the metal-AF transition, similar to the one we perform here, would be useful to undertake.

QMC vs. ED.— A valuable test of the conjecture that $\langle S \rangle$ tracks a quantum phase transition (or regime) can be made by comparing QMC results with exact ones, obtained at smaller lattice sizes. For this purpose, we contrast in Fig. S4 the average sign in a lattice with $L = 4$ with numerical results obtained from exact diagonalization (ED). At this small lattice size, the quantum critical region shrinks, and at the lowest temperatures studied ($T/t = 1/24$) $\langle S \rangle$ displays a sharp dip at around $V/t \simeq 2$. Turning to the ED results, we probe the transition via the analysis of the low lying spectrum E_α (E_0 is the ground-state), the many-body excitation gaps $\Delta_{\text{ex}}^{(\alpha)} = E_\alpha - E_0$, the spin and charge staggered structure factors, $S_{\text{sdw}} = (1/N) \sum_{i,j} (-1)^\eta \langle (n_{i\uparrow} - n_{i\downarrow})(n_{j\uparrow} - n_{j\downarrow}) \rangle$ and $S_{\text{cdw}} = (1/N) \sum_{i,j} (-1)^\eta \langle (n_{i\uparrow} + n_{i\downarrow})(n_{j\uparrow} + n_{j\downarrow}) \rangle$ [$\eta = +1$ (-1) when i, j belong to the same (different) sublattices], and, the fidelity metric $g_U = \frac{2}{N} \frac{1 - |\langle \Psi_0(U) | \Psi_0(U+dU) \rangle|}{dU^2}$. This last quantity displays a peak whenever one crosses a quantum phase transition for the parameters U and $U + dU$. These results describe a single transition in the range of parameters investigated, displaying a first-order character, given the level crossings shown in Fig. S4(B) or a vanishing excitation gap $\Delta_{\text{ex}}^{(1)} = E_1 - E_0$ at $U/t \simeq 1.99$ [Fig. S4(C)]. In turn, the fidelity metric displays a sharp peak at this interaction value [Fig. S4(E)], and the structure factors computed at the ground-state swap its characteristics, from a charge- to a spin-ordered one [Fig. S4(D)]. It is an open question of whether one is able to capture the intermediate correlated metal phase in exact methods such as ED.

Stepping back from the technical details, the central message of Fig. S4 is extending the evidence presented in the main text that the sign problem metric for the QCP of panel A lines up well with those of the ‘traditional observables’ in panels B-E.

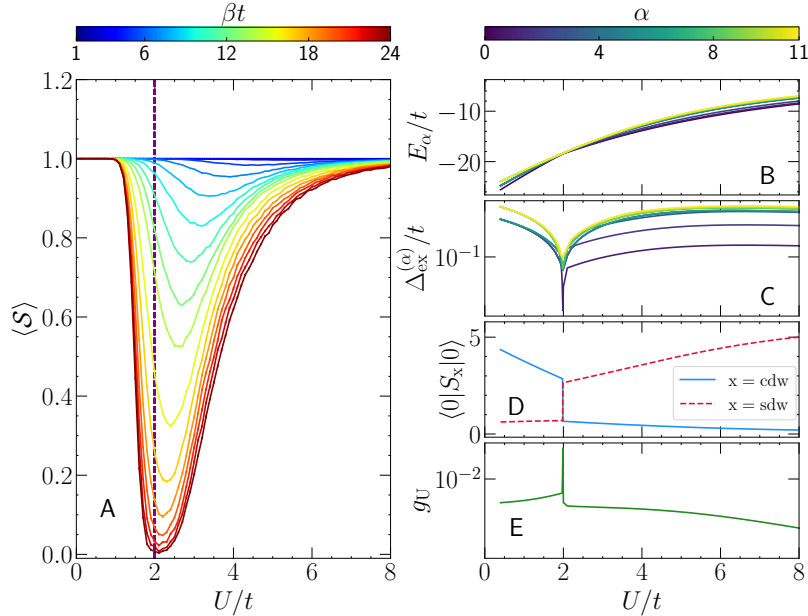


Figure S4. **QMC vs. ED on a 4×4 lattice.** (A) The average sign extracted from the DQMC calculations $\langle S \rangle$ for increasing inverse temperatures $\beta = 1/T$ as a function of the Hubbard interaction U/t in a lattice with $L = 4$ and a staggered potential $\Delta/t = 0.5$. (B–E) Data extracted with the ED, including: (B) The low-lying eigenspectrum E_α at the zero-momentum sector $\mathbf{k} = (0, 0)$; (C) The excitation gaps $\Delta_{\text{ex}}^{(\alpha)}$; (D) the spin and charge structure factors and (E) the fidelity metric under variations of the interaction magnitudes U , using $dU = 10^{-3}t$. In (A), data are averaged over 24 independent runs, with $\Delta\tau = 0.1$.

MORE DETAILS ON SPINLESS HONEYCOMB HUBBARD (MAIN TEXT, SEC. III)

The finite-temperature transition.— As we have argued in the main text, the interacting spinless fermion Hamiltonian has a special property in AFQMC simulations: with an appropriate choice of the basis one uses to write the fermionic matrix, it has been proven that the sign problem can be eliminated [34, 38, 41]. Nonetheless, using a standard single-particle basis, where the sign problem is manifest, we demonstrated in Fig. 3 that $\langle \mathcal{S} \rangle$ can be used as a way to track the quantum phase transition. Concomitantly, we have shown that a local observable (the derivative of the nearest neighbor density correlations with respect to the interactions V) exhibits a steep downturn once the quantum (i.e. zero temperature) phase transition is approached.

As a by-product of this analysis, we use our original approach based on the standard BSS algorithm in the standard fermionic basis to show that one can also obtain an estimation of the *finite-temperature* transition (pertaining to universality class of the 2D Ising model) with a relatively large accuracy, if the system is not too close to the quantum critical point, see Fig. S5. We compute both the derivative of the nearest-neighbor density correlations as well as the CDW structure factor, i.e., a summation of all density-density correlations with a +1 (−1) for sites belonging to the same (different) sublattice, on the largest lattice size we have investigated, $L = 18$. These finite-size results for T_c are in good agreement with recent results obtained after system size scaling of data extracted with continuous-time QMC methods [22, 48], where the sign problem is absent.

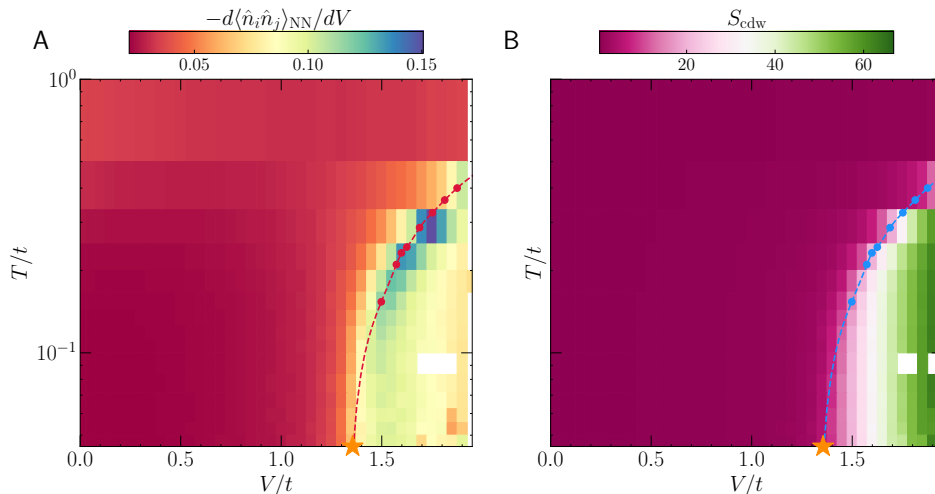


Figure S5. **Finite-temperature transition for the spinless fermion on the honeycomb lattice.** As a by-product of the analysis of the temperature dependence for average sign, we notice that other than in regimes very close to the QCP, $\langle \mathcal{S} \rangle$ is very close to 1. (A) The derivative of the nearest-neighbor density correlations in the T/t vs. V/t plane and (B) the CDW structure factor for a lattice with $L = 18$. In both plots, the markers are the continuous-time QMC results extracted after finite-size scaling in Ref. [48]. Imaginary-time discretization is fixed at $\Delta\tau = 0.1$, and all data is obtained as an average of 20 independent runs.

An important outcome of these results is that they imply that the mark that a phase transition leaves on the average sign is restricted to quantum phase transitions, rather than thermal ones, as we show above.

Imaginary-time discretization.— Here we consider the effect of the imaginary-time discretization $\Delta\tau$ on the average sign, for a fixed inverse temperature and show that ‘Trotter errors’ [159] do not affect our conclusions. Figure S6 shows the average sign for a fixed lattice size $L = 9$ and $\Delta\tau$ ranging from 0.025 to 0.2 with a fixed temperature $T/t = 1/24$. The drop in $\langle \mathcal{S} \rangle$ when approaching V_c is indicative of the QCP, but using a more dense imaginary-time discretization does not render substantial changes in the average sign; similar behavior was observed in other models studied.

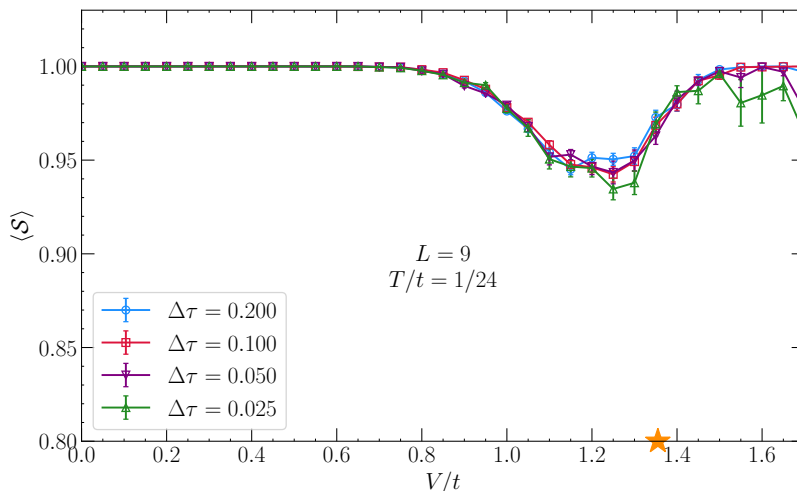


Figure S6. **The U(1) model on the honeycomb lattice: Average sign dependence on the imaginary time-discretization.** The dependence of $\langle \mathcal{S} \rangle$ on the imaginary-time discretization $\Delta\tau$ with growing interactions V/t , in a lattice with $L = 9$. Data is extracted as an average of 24 independent runs, for a temperature $T/t = 1/24$. The best known value for the Mott insulating transition [41] ($V_c/t = 1.355$) is signalled by the star marker.

MORE DETAILS FOR THE HOMOGENEOUS HUBBARD MODEL ON THE SQUARE LATTICE (MAIN TEXT, SEC. IV)

Finite-size effects.— An important aspect that deserves further attention concerns finite-size effects on the data presented in the main text. The average sign, for example, when not protected by some underlying symmetry of the Hamiltonian, is known to decrease for larger system sizes [29]. Figure S7 compares the original quantities displayed in the main text [Fig. 4] at different lattice sizes. The “growth” of the $\langle \mathcal{S} \rangle \rightarrow 0$ dome is relatively small when taking into account lattices differing by an order of magnitude in the number of sites. The d -wave pair-susceptibility also qualitatively preserves its overall features, with a tendency of local pair formation at higher electronic densities, encapsulating the $\langle \mathcal{S} \rangle \rightarrow 0$ dome. Similarly, the static spin-susceptibility and its accompanying ‘pseudogap’ line are largely unaltered when the linear lattice size varies from $L = 8$ to 16. These results for different L indicate that our analysis of the link between the SP and quantum criticality is not a finite size effect.

Pair-symmetry channels.— Another important check on the suitability of the chosen parameters to describe the physics of pairs with the same experimentally inferred symmetry as in the cuprates, is to directly compare the correlated susceptibility map with different symmetry channels. This has been done in early studies of QMC [57], and here, as a side-aspect of the analysis of the average sign, we bring in a systematic investigation. Figure S8 displays the correlated pair susceptibility $\langle P_\alpha - P_\alpha^{\text{nv}} \rangle$ dependence on the temperature and electronic filling, with $\alpha = d, s^*$ or s -wave. Clearly, the symmetric local pairing channel (s -wave), which directly confronts the on-site U , is not favored in the whole range of T and ρ investigated. The correlated pair susceptibility is always negative for finite values of $\langle \mathcal{S} \rangle$, indicating the vertex is *repulsive*. In contrast, both the extended s -wave and d -wave pairings exhibit positive correlated pairing susceptibilities in the vicinity of the $\langle \mathcal{S} \rangle \rightarrow 0$ dome, but are more pronounced in the latter. This emphasizes the dominance of d -wave pairing in the Hubbard model, in direct analogy to a wide class of materials displaying high-temperature superconductivity.

Spectral weight at the anti-nodal point.— In describing the physics of cuprates, a common focus is the anisotropy of the single-particle gap as extracted from ARPES techniques [49], which contrasts with the standard isotropic behavior seen in conventional BCS-type superconductors. At the root of the discussion is the shape of the Fermi surface when doping the parent spin-ordered Mott insulator. In particular, to classify the onset of the pseudogap phase at low enough temperatures T , i.e., the regime where single-particle, low-energy excitations are suppressed, one tracks the peak of the anti-nodal spectral weight at the Fermi energy, $A_{(\pi,0)}(\omega = 0) \equiv -\frac{1}{\pi} \text{Im}G_{(\pi,0)}(\omega = 0)$ as T is varied.

In QMC simulations, this quantity can in principle be extracted by means of an analytical continuation of the data, in which the imaginary-time dependence of the Green’s function G is converted to real frequency. To avoid the well known difficulty of such a calculation [162], a proxy valid at low enough temperatures, $A_{(\pi,0)}^{\text{proxy}} = \beta G_{(\pi,0)}(\tau = \beta/2)$ is often used [163, 164]. Figure S9 shows the results for the anti-nodal spectral function. The pseudogap line extracted

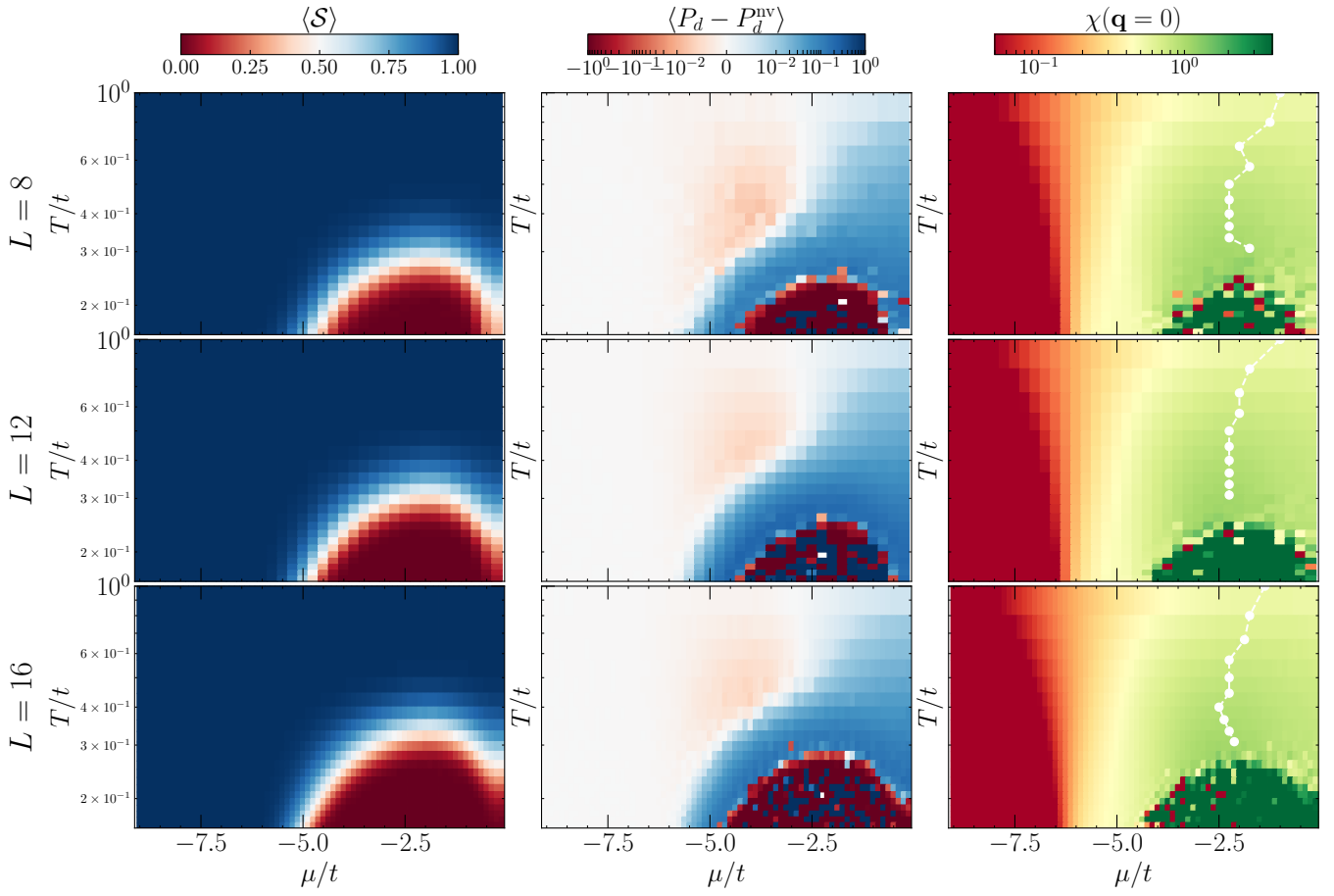


Figure S7. **Finite size effects for the SU(2) Hubbard model on the square lattice.** An analysis of the main quantities and their size dependence for the model with potential connection with the physics of the cuprates. As in the main text, we choose $U/t = 6$ and $t'/t = -0.2$. The top, middle, and bottom rows of plots refer to $L = 8, 12$ and 16 , respectively. In turn, the columns from left to right depict the average sign, the correlated d -wave pair susceptibility, and the long-wavelength static spin susceptibility. Imaginary-time discretization is fixed at $\Delta\tau = 0.0625$, and all data are extracted as an average of 24 independent runs.

from the proxy is qualitatively close to the one obtained from the peak of the static long-wavelength spin susceptibility (Figs. 4 and S7) and, like it, terminates on the $\langle \mathcal{S} \rangle \rightarrow 0$ dome.

Spectral function and the Lifshitz transition.— The extensive dataset and associated analysis we have undertaken in this investigation of the sign problem enables us to check other important physical aspects of the Hubbard model on the square lattice, and their relation to cuprate phenomenology. We include them here, in order to further link their behavior to that of the sign. One of them refers to the change of the topology of the Fermi surface when increasing the hole-doping (decreasing the electron density) from half-filling: at some critical $\langle n \rangle$, the Fermi surface changes its shape from hole-like to a closed, electron-like one. This transition, referred to as the Lifshitz transition, has been investigated in the context of strongly interacting electrons, and was inferred to occur concomitantly with the presence of a van Hove singularity at the Fermi level [165].

Due to the presence of the SP, however, we can only investigate the Lifshitz transition at finite-temperatures, and thus the Fermi ‘surface’ is thermally broadened. Nonetheless, Fig. S10 displays the spectral function (obtained via the ‘proxy’ scheme as previously explained) at the Fermi energy on lattices with linear size $L = 24$, at a temperature right above the $\langle \mathcal{S} \rangle \rightarrow 0$ dome, and investigating dopings above and below the pseudogap line in Figs. 4 and S10. As one increases the density, the change of topology precisely confirms the Lifshitz-scenario, with a further formation of hole-pocket regions along the anti-nodal direction, in direct analogy to the phenomenology of high- T_c superconductors [49].

Comparison to the near-neighbor hopping only Hubbard model.— While it is remarkable how much of the physics of simplest Hubbard Hamiltonian captures that of the cuprates [58], refinements of the model are known to provide more accurate comparisons to the experiments [160, 161, 166]. One such, the inclusion of next-nearest neighbor

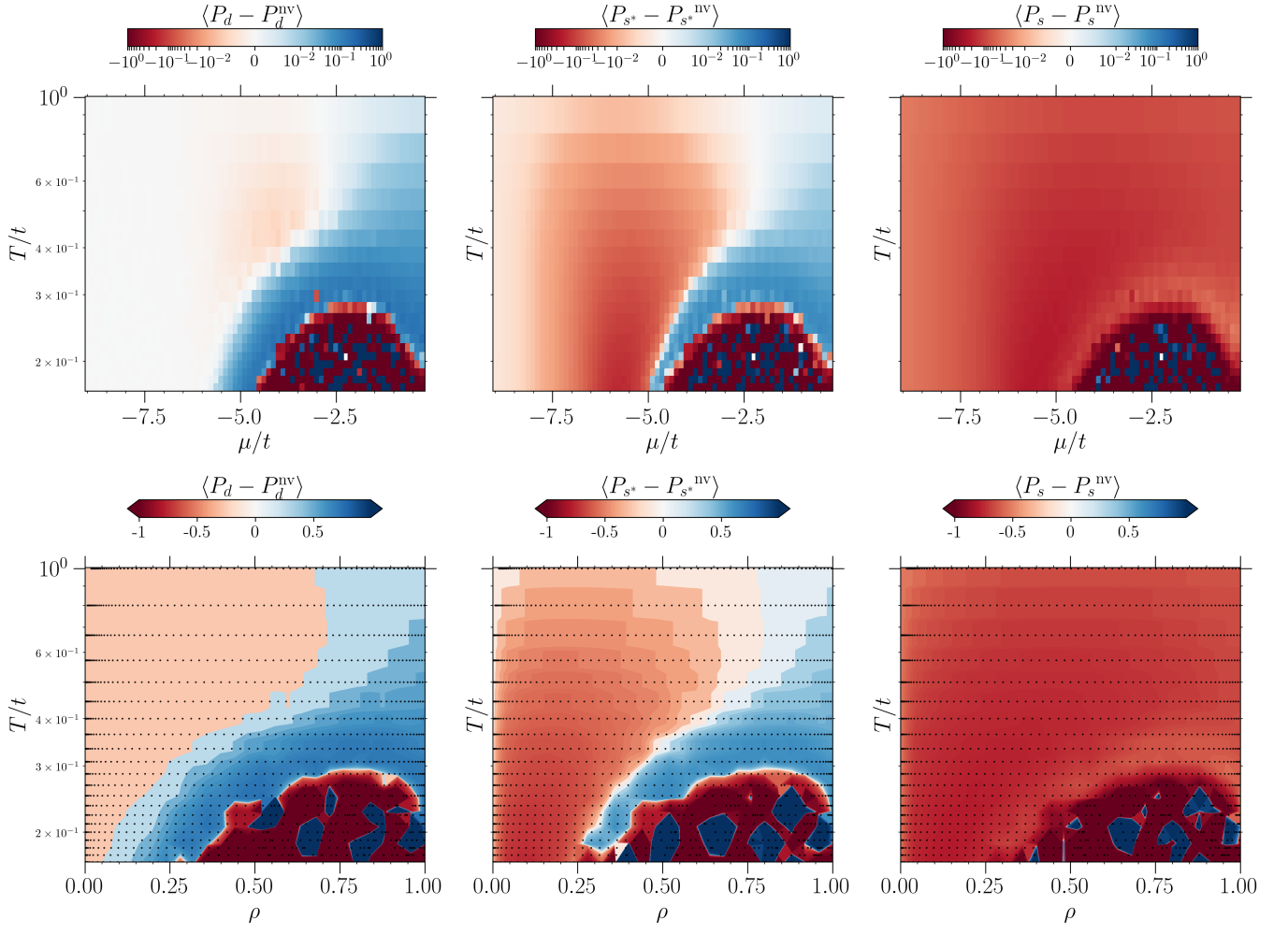


Figure S8. **Comparison of the pairing channels for the SU(2) Hubbard model on the square lattice.** Taking as a starting point for the physics of the cuprates the parameters $U/t = 6$ and $t'/t = -0.2$ [160, 161], we display the comparison of the correlated pair susceptibilities considering different symmetry channels in the left (d -wave), center (extended s -wave, s^*) and right (s -wave) columns, both in μ/t vs. T/t (upper row) and ρ vs. T/t (lower row) parametric space. Imaginary-time discretization is fixed at $\Delta\tau = 0.0625$, and all data are extracted as an average of 24 independent runs in a lattice with $L = 16$.

hopping t' was employed in the analysis in the main text. It is significant in the context of the sign problem because it breaks the particle-hole symmetry and, for example, induces a SP even at half-filling. In this section we address the extent to which including t' affects our conclusions. To this end, we contrast the results of Fig. 4 with the ones arising from the Hubbard model with $t' = 0$ (Fig. S11). The key qualitative aspects are similar, including the presence of a $\langle \mathcal{S} \rangle \rightarrow 0$ dome, the tendency of d -wave pair formation (due to the enhanced pair susceptibility with this symmetry around such dome) and a peak of the spin susceptibility ending at the dome. The differences are: (i) while approaching half-filling, the average sign displays a sudden jump towards 1 (as one would expect for this bipartite case), (ii) the extension of the dome, within the temperatures investigated ($T/t \geq 1/6$), is more constrained in density compared to the $t'/t = -0.2$ case, and, more importantly, (iii) the pseudogap region, signified by the temperatures below the $\chi(\mathbf{q} = 0)$ peak, is significantly reduced. Our data thus provide another argument in support of an added next-nearest neighbor hopping in order to possibly explain the phase diagram of high T_c materials, which display a robust pseudogap region. However, the main point for the purpose of this manuscript is that whether t' is included or not, the behavior of the sign is correlated with the physics of pairing and magnetism.

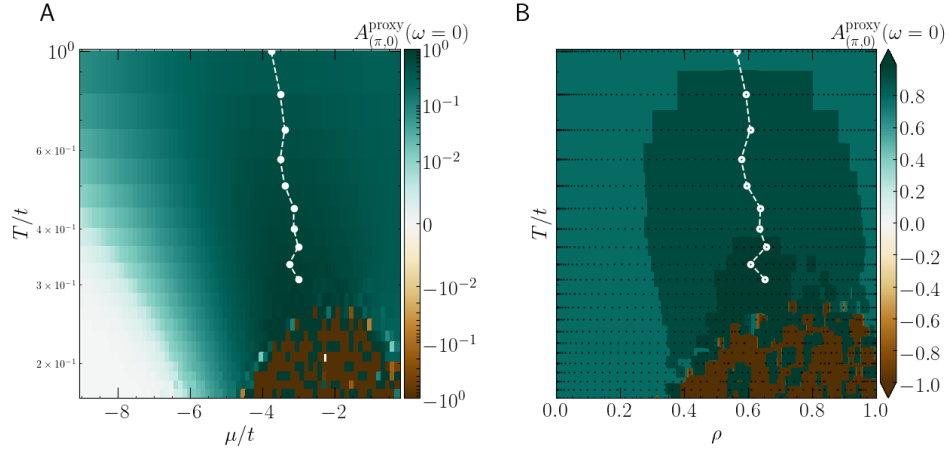


Figure S9. **Comparison of the single-particle spectral weight at the anti-nodal point.** Temperature extrapolation of the extracted $A_{(\pi,0)}$ at the Fermi energy vs the chemical potential μ/t (A) and the electronic density ρ (B), on a lattice with $L = 16$; other parameters are $U/t = 6$ and $t'/t = -0.2$. The maximum values at each temperature are denoted by the white markers. Imaginary-time discretization is fixed at $\Delta\tau = 0.0625$, and all data is extracted as an average of 24 independent runs.

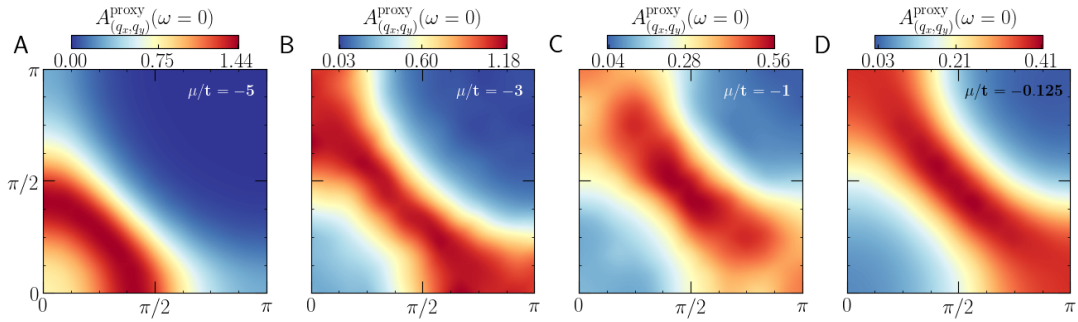


Figure S10. **Lifshitz transition.** The evolution of the spectral function in one quadrant of the Brillouin zone with increasing densities, after an interpolation of the results for a 24×24 lattice at temperature $T/t = 1/3.25$, with $U/t = 6$ and $t'/t = -0.2$. The different panels depict results with various chemical potentials as marked, and the average density is 0.25 in (A), 0.65 in (B), 0.95 in (C), and 1.00 in (D). Imaginary-time discretization is fixed at $\Delta\tau = 0.0625$, and all data is extracted as an average of 20 independent runs.

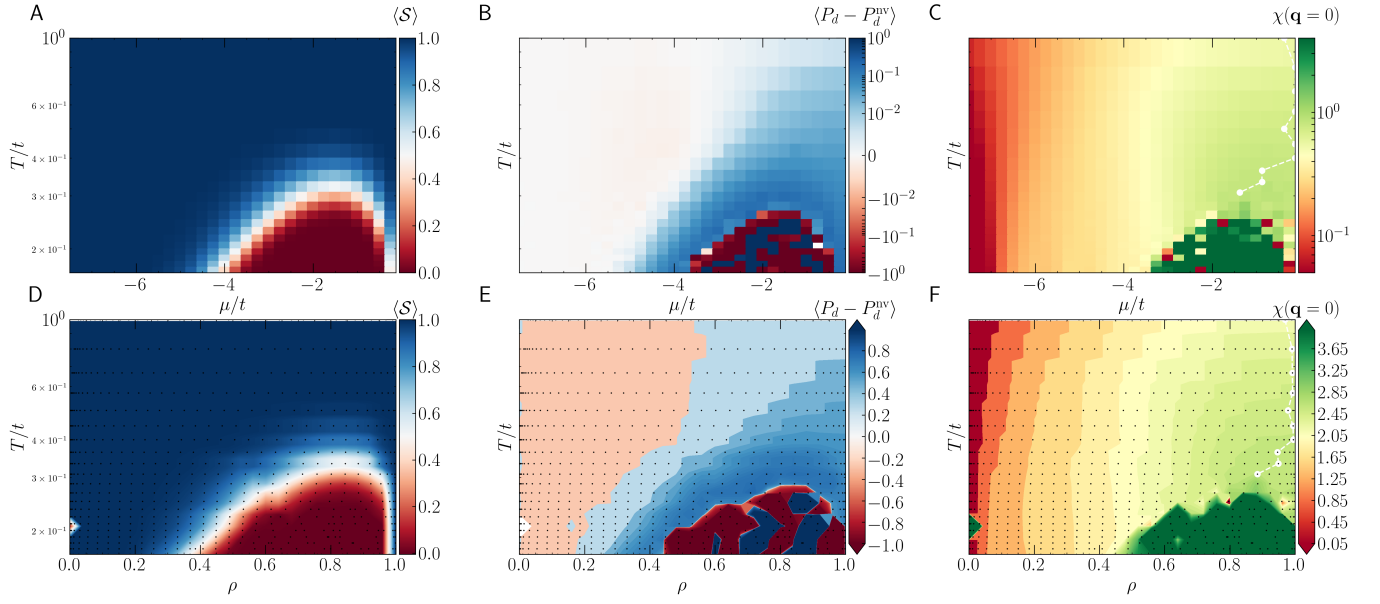


Figure S11. The ‘phase diagram’ of the bipartite Hubbard model on the square lattice. The same as Fig. 4 in the main text, but instead removing the non-bipartite contribution t' , i.e., here the ‘vanilla’ Hubbard model results are presented. Other parameters are the same, as $L = 16$, $\Delta\tau = 0.0625$ and $U/t = 6$.